TABLE 2. Influx Ratios and Volumes of Thalamic Subregions in Patients With Schizophrenia and Healthy Comparison Subjects

	Influx Ratio[a]						Volume (cm^3)					
	Healthy Subjects (N=19)		Schizophrenia Patients (N=10)		Analysis of Variance		Healthy Subjects (N=19)		Schizophrenia Patients (N=10)		Analysis of Covariance[b]	
Thalamic Subregion	Mean	SD	Mean	SD	F (df=1, 27)	p	Mean	SD	Mean	SD	F (df=1, 26)	p
Anterior medial	0.87	0.06	0.83	0.07	2.20	0.15	2.25	0.38	2.29	0.32	0.05	0.83
Anterior lateral	0.80	0.08	0.77	0.08	1.32	0.26	0.80	0.25	0.77	0.28	0.11	0.75
Central medial	0.92	0.08	0.88	0.04	1.38	0.25	2.39	0.51	2.27	0.50	0.29	0.59
Central lateral	0.90	0.06	0.87	0.06	2.07	0.16	1.89	0.41	1.93	0.33	0.02	0.89
Posterior	0.80	0.06	0.78	0.05	0.60	0.45	1.33	0.23	1.39	0.26	0.37	0.55

[a] The ratio of radioligand delivery in the region of interest to that in the reference region (cerebellum).
[b] Intracranial volume entered as covariate.

TABLE 3. Correlations Between [^{11}C]FLB457 Binding Potential[a] and BPRS Total and Positive and Negative Symptom Scores in Patients With Schizophrenia (N=10)

	Correlation Between Binding Potential and BPRS Score					
	Total Scale		Positive Symptoms		Negative Symptoms	
Thalamic Subregion	r	p	r	p	r	p
Anterior medial	−0.06	0.86	−0.18	0.62	0.23	0.52
Anterior lateral	0.06	0.88	0.39	0.27	−0.41	0.24
Central medial	−0.64	0.05	−0.78	0.008	0.01	0.97
Central lateral	−0.03	0.93	−0.11	0.77	0.31	0.38
Posterior	−0.58	0.08	−0.80	0.006	0.18	0.61

[a] Index of dopamine D_2 receptor binding.

FIGURE 3. Relationship Between [^{11}C]FLB457 Binding Potential in the Central Medial and Posterior Subregions of the Thalamus and BPRS Positive Symptom Score in Patients With Schizophrenia (N=10)

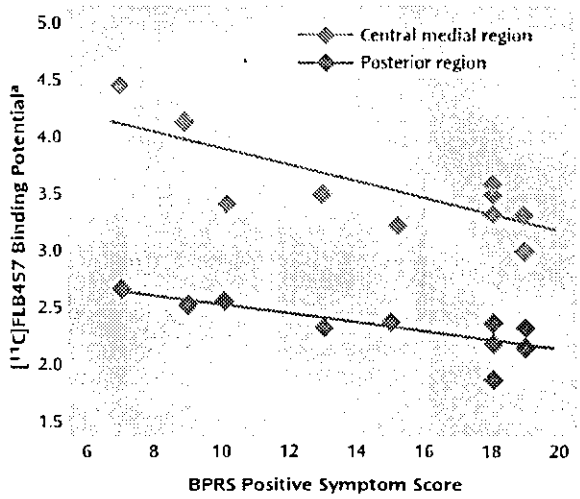

[a] Index of dopamine D_2 receptor binding.

agonist apomorphine into the medial thalamus (43). The dorsomedial nucleus has connections to the prefrontal cortex and anterior cingulate (44). Both these regions have also been included in discussions on the gating function (39). An abnormality of the dorsomedial nucleus in schizophrenia may be attributed to functional disturbances in any of the brain regions discussed in relation to sensory gating.

The other subnuclei with low binding potential are found in the pulvinar. This is one of several structures implicated in attentional processing and salience (45–47). The pulvinar has connections with the visual and auditory cortex as well as the prefrontal cortex and temporal association areas (48). A primary abnormality in the pulvinar may thus induce unusual associations and sensory disturbances in schizophrenia (26). Taken together, these two regions may have a functional role consistent with several of the disturbed functions in schizophrenia and underlie the correlation with BPRS positive symptom score.

The observation of a significant negative correlation between subregional binding potential and positive symptom score is similar to that previously reported for [^{11}C]FLB457 binding in the anterior cingulate. The anterior cingulate has direct connections with the dorsomedial nucleus and the pulvinar (48–50). When we examined the relationship between dopamine D_2 receptor binding in the central medial and posterior regions of the thalamus and that of the anterior cingulate using the Pearson correlation method, we found a significant interrelationship between those regions in patients with schizophrenia ($p<0.05$). The abnormality shown in the thalamic subregions might have a similar background to that in the anterior cingulate. However, the cellular localization of D_2 receptors in the thalamic subregions that might allow speculation about the altered regulatory function of interneurons with D_2 receptors has not yet been determined, as discussed in the previous study (1).

Reduced regional blood flow has been reported in the thalamus of schizophrenia (51). However, the reduction of binding potential is unlikely to be a result of altered blood flow, since the R_1 value did not differ significantly between the healthy subjects and patients. While morphological changes have been reported in the thalamic mediodorsal nucleus and pulvinar in schizophrenia (7, 8), and this can affect binding potential, no significant difference was observed in the volumes of thalamic subdivisions, including the central medial and posterior regions, between our examined patient and comparison groups. The relatively moderate severity and short duration of illness in our pa-

tient group may explain the lack of volume change (52, 53). In any case, low dopamine D_2 receptor binding can therefore not be attributed to reductions in gross brain anatomy.

There are several confounding factors in this study. First, the number of patients was small, raising the question of adequate statistical power, and thus it cannot be ruled out that a larger study population might reveal that the binding potential values of other thalamic subregions and volumetric measurements will also show significant differences. In addition, [^{11}C]FLB457 has high affinity not only for dopamine D_2 receptors but also for dopamine D_3 receptors (27). Dopamine D_3 receptors are distributed mainly to the ventral striatum and the islands of Calleja in the postmortem human brain, but they have as yet not been distinctly identified in the thalamus (54–56). Thus, there is a possibility that our findings could be partly explained by the reduction of dopamine D_3 receptors, but this will have to await the outcome of future studies on the amount of dopamine D_3 receptors in the thalamus. Another factor is that psychopathology was assessed by the 18-item BPRS, but this scale mainly measures the affective component of the negative symptoms and does not cover well the additional components that identify cognitive, anergic, and social dimensions (57).

Finally, our measurement of thalamic subdivisions has several limitations. We were unable to delineate and employ an intrathalamic marker as a consistent landmark for our regional subdivisions. Rather, we relied upon approximate percentage-based divisions of the total thalamic area as a means of dividing the thalamus. This automated method reduced some of the subjectivity and systematic bias involved in defining subthalamic areas with limited resolution imaging. However, without manual editing, the assumptions that all thalamic nuclei are consistently represented by these rigid subdivisions cannot be assured, and the volume of each subdivision would not be comparable with data from carefully edited volumetric studies.

Received Jan. 7, 2003; revisions received May 6 and Oct. 7, 2003; accepted Oct. 9, 2003. From the Brain Imaging Project, National Institute of Radiological Sciences, Chiba, Japan; CREST Japan Science and Technology Corporation, Saitama, Japan; Biofunctional Informatics, Graduate School of Allied Health Sciences, Tokyo Medical and Dental University, Tokyo, Japan; the Department of Psychiatry, Jikei University School of Medicine, Tokyo, Japan; and the Psychiatry Section, Department of Clinical Neuroscience, Karolinska Institute, Stockholm, Sweden. Address reprint requests to Dr. Suhara, Brain Imaging Project, National Institute of Radiological Sciences, 4–9–1 Anagawa, Inage-ku, Chiba 263–8555, Japan; suhara@nirs.go.jp (e-mail).

Supported by the PET project of the National Institute of Radiological Sciences in Chiba, Japan.

The authors thank T. Saijo, T. Ando, A. Yamamoto, Y. Asai, S. Ito, and T. Nakayama for their help in data acquisition and N. Kinukawa for discussions and comments about the statistics.

References

1. Suhara T, Okubo Y, Yasuno F, Sudo Y, Inoue M, Ichimiya T, Nakashima Y, Nakayama K, Tanada S, Suzuki K, Halldin C, Farde L: Decreased dopamine D2 receptor binding in the anterior cingulate cortex in schizophrenia. Arch Gen Psychiatry 2002; 59:25–30
2. Andreasen NC, Arndt S, Swayze V II, Cizadlo T, Flaum M, O'Leary D, Ehrhardt JC, Yuh WTC: Thalamic abnormalities in schizophrenia visualized through magnetic resonance image averaging. Science 1994; 266:294–298
3. Andreasen NC, Ehrhardt JC, Swayze VW II, Alliger RJ, Yuh WT, Cohen G, Ziebell S: Magnetic resonance imaging of the brain in schizophrenia: the pathophysiologic significance of structural abnormalities. Arch Gen Psychiatry 1990; 47:35–44
4. Pakkenberg B: The volume of the mediodorsal thalamic nucleus in treated and untreated schizophrenics. Schizophr Res 1992; 7:95–100
5. Buchsbaum MS, Someya T, Teng CY, Abel L, Chin S, Najafi A, Haier RJ, Wu J, Bunney WE Jr: PET and MRI of the thalamus in never-medicated patients with schizophrenia. Am J Psychiatry 1996; 153:191–199
6. Gur RE, Maany V, Mozley PD, Swanson C, Bilker W, Gur RC: Subcortical MRI volumes in neuroleptic-naive and treated patients with schizophrenia. Am J Psychiatry 1998; 155:1711–1717
7. Gilbert AR, Rosenberg DR, Harenski K, Spencer S, Sweeney JA, Keshavan MS: Thalamic volumes in patients with first-episode schizophrenia. Am J Psychiatry 2001; 158:618–624
8. Byne W, Buchsbaum MS, Kemether E, Hazlett EA, Shinwari A, Mitropoulou V, Siever LJ: Magnetic resonance imaging of the thalamic mediodorsal nucleus and pulvinar in schizophrenia and schizotypal personality disorder. Arch Gen Psychiatry 2001; 58:133–140
9. Ananth H, Popescu I, Critchley HD, Good CD, Frackowiak RSJ, Dolan RJ: Cortical and subcortical gray matter abnormalities in schizophrenia determined through structural magnetic resonance imaging with optimized volumetric voxel-based morphometry. Am J Psychiatry 2002; 159:1497–1505
10. Rodriguez VM, Andree RM, Castejon MJ, Zamora ML, Alvaro PC, Delgado JL, Vila FJ: Fronto-striato-thalamic perfusion and clozapine response in treatment-refractory schizophrenic patients: a 99mTc-HMPAO study. Psychiatry Res 1997; 76:51–61
11. Holcomb HH, Cascella NG, Thaker GK, Medoff DR, Dannals RF, Tamminga CA: Functional sites of neuroleptic drug action in the human brain: PET/FDG studies with and without haloperidol. Am J Psychiatry 1996; 153:41–49
12. Heimberg C, Komoroski RA, Lawson WB, Cardwell D, Karson CN: Regional proton magnetic resonance spectroscopy in schizophrenia and exploration of drug effect. Psychiatry Res 1998; 83:105–115
13. Gunther W: MRI-SPECT and PET-EEG findings on brain dysfunction in schizophrenia. Prog Neuropsychopharmacol Biol Psychiatry 1992; 16:445–462
14. Pakkenberg B: Pronounced reduction of total neuron number in mediodorsal thalamic nucleus and nucleus accumbens in schizophrenics. Arch Gen Psychiatry 1990; 47:1023–1028
15. Young KA, Manaye KF, Liang C, Hicks PB, German DC: Reduced number of mediodorsal and anterior thalamic neurons in schizophrenia. Biol Psychiatry 2000; 47:944–953
16. Popken GJ, Bunney WE Jr, Potkin SG, Jones EG: Subnucleus-specific loss of neurons in medial thalamus of schizophrenics. Proc Natl Acad Sci USA 2000; 97:9276–9280
17. Byne W, Buchsbaum MS, Mattiace LA, Hazlett EA, Kemether E, Elhakem SL, Purohit DP, Haroutunian V, Jones L: Postmortem assessment of thalamic nuclear volumes in subjects with schizophrenia. Am J Psychiatry 2002; 159:59–65
18. Blennow K, Bogdanovic N, Heilig M, Grenfeldt B, Karlsson I, Davidsson P: Reduction of the synaptic protein rab3a in the thalamus and connecting brain regions in post-mortem schizophrenic brains. J Neural Transm 2000; 107:1085–1097

19. Ungerstedt U: Stereotaxic mapping of monoamine pathways in the rat brain. Acta Physiol Scand 1971; 367:1–48
20. Kessler RM, Whetsell WO, Ansari MS, Votaw JR, de Paulis T, Clanton JA, Schmidt DE, Mason NS, Manning RG: Identification of extrastriatal dopamine D2 receptors in post mortem human brain with [125I]epidepride. Brain Res 1993; 609:237–243
21. Langer O, Halldin C, Dolle F, Swahn CG, Olsson H, Karlsson P, Hall H, Sandell J, Lundkvist C, Vaufrey F, Loc'h C, Crouzel C, Maziere B, Farde L: Carbon-11 epidepride: a suitable radioligand for PET investigation of striatal and extrastriatal dopamine D2 receptors. Nucl Med Biol 1999; 26:509–518
22. Sedvall G, Farde L: Chemical brain anatomy in schizophrenia. Lancet 1995; 346:743–749
23. Suhara T, Sudo Y, Okauchi T, Maeda J, Kawabe K, Suzuki K, Okubo Y, Nakashima Y, Ito H, Tanada S, Halldin C, Farde L: Extrastriatal dopamine D2 receptor density and affinity in the human brain measured by 3D PET. Int J Neuropsychopharmacol 1999; 2:73–82
24. Okubo Y, Olsson H, Ito H, Lofti M, Suhara T, Halldin C, Farde L: PET mapping of extrastriatal D2-like dopamine receptors in the human brain using an anatomic standardization technique and [11C]FLB 457. Neuroimage 1999; 10:666–674
25. Farde L, Suhara T, Nyberg S, Karlsson P, Nakashima Y, Hietala J, Halldin C: A PET-study of [11C]FLB 457 binding to extrastriatal D2-dopamine receptors in healthy subjects and antipsychotic drug-treated patients. Psychopharmacology (Berl) 1997; 133: 396–404
26. Jones EG: The Thalamus. New York, Plenum, 1985
27. Halldin C, Farde L, Hogberg T, Mohell N, Hall H, Suhara T, Karlsson P, Nakashima Y, Swahn CG: Carbon-11-FLB 457: a radioligand for extrastriatal D2 dopamine receptors. J Nucl Med 1995; 36:1275–1281
28. Kitamura T, Machizawa S, Maruyama S, Nakagawa Y, Morita M, Sato T: Test-retest reliability of Oxford University version of the Brief Psychiatric Rating Scale (BPRS): a preliminary survey of multicenter collaborative study initiated by the National Institute of Mental Health. J Ment Health 1985; 32:1–15
29. Kane J, Honigfeld G, Singer J, Meltzer H: Clozapine for the treatment-resistant schizophrenic: a double-blind comparison with chlorpromazine. Arch Gen Psychiatry 1988; 45:789–796
30. Lammertsma AA, Hume S: Simplified reference tissue model for PET receptor studies. Neuroimage 1996; 4:153–158
31. Olsson H, Halldin C, Swahn CG, Farde L: Quantification of [11C]FLB 457 binding to extrastriatal dopamine receptors in the human brain. J Cereb Blood Flow Metab 1999; 19:1164–1173
32. Mintun MA, Raichle ME, Kilbourn MR, Wooten GF, Welch MJ: A quantitative model for the in vivo assessment of drug binding sites with positron emission tomography. Ann Neurol 1984; 15:217–227
33. Yasuno F, Hasnine AH, Suhara T, Ichimiya T, Sudo Y, Inoue M, Takano A, Ou T, Ando T, Toyama H: Template-based method for multiple volumes of interest of human brain PET images. Neuroimage 2002; 16:577–586
34. Friston KJ, Holmes AP, Worsley KJ, Poline JP, Frith CD, Frackowiak RSJ: Statistical parametric maps in functional imaging: a general linear approach. Hum Brain Mapp 1995; 2:189–210
35. Studholme C, Hill DL, Hawkes DJ: Automated three-dimensional registration of magnetic resonance and positron emission tomography brain images by multiresolution optimization of voxel similarity measures. Med Phys 1997; 24:25–35
36. Oke AF, Adams RN: Elevated thalamic dopamine: possible link to sensory dysfunctions in schizophrenia. Schizophr Bull 1987; 13:589–604
37. Okauchi T, Suhara T, Maeda J, Kawabe K, Obayashi S, Suzuki K: Effect of endogenous dopamine on extrastriatal [11C]FLB 457 binding measured by PET. Synapse 2001; 41:87–95
38. Goldsmith SK, Shapiro RM, Joyce JN: Disrupted pattern of D2 dopamine receptors in the temporal lobe in schizophrenia. Arch Gen Psychiatry 1997; 54:649–658
39. Carlsson A, Waters N, Waters S, Carlsson ML: Network interactions in schizophrenia—therapeutic implications. Brain Res Brain Res Rev 2000; 31:342–349
40. Perry W, Feifel D, Minassian A, Bhattacharjie I, Braff DL: Information processing deficits in acutely psychotic schizophrenia patients medicated and unmedicated at the time of admission. Am J Psychiatry 2002; 159:1375–1381
41. Hazlett EA, Buchsbaum MS, Haznedar MM, Singer MB, Germans MK, Schnur DB, Jimenez EA, Buchsbaum BR, Troyer BT: Prefrontal cortex glucose metabolism and startle eyeblink modification abnormalities in unmedicated schizophrenia patients. Psychophysiology 1998; 35:186–198
42. Kodsi MH, Swerdlow NR: Regulation of prepulse inhibition by ventral pallidal projections. Brain Res Bull 1997; 43:219–228
43. Young KA, Randall PK, Wilcox RE: Startle and sensorimotor correlates of ventral thalamic dopamine and GABA in rodents. Neuroreport 1995; 6:2495–2499
44. Jones EG: Cortical development and thalamic pathology in schizophrenia. Schizophr Bull 1997; 23:483–501
45. Robinson DL, Petersen SE: The pulvinar and visual salience. Trends Neurosci 1992; 15:127–132
46. LaBerge D, Buchsbaum MS: Positron emission tomographic measurements of pulvinar activity during an attention task. J Neurosci 1990; 10:613–619
47. Morris JS, Friston KJ, Dolan RJ: Neural responses to salient visual stimuli. Proc R Soc Lond B Biol Sci 1997; 264:769–775
48. Romanski LM, Giguere M, Bates JF, Goldman-Rakic PS: Topographic organization of medial pulvinar connections with the prefrontal cortex in the rhesus monkey. J Comp Neurol 1997; 379:313–332
49. Vogt BA, Pandya DN, Rosene DL: Cingulate cortex of the rhesus monkey, I: cytoarchitecture and thalamic afferents. J Comp Neurol 1987; 262:256–270
50. Vogt BA, Pandya DN: Cingulate cortex of the rhesus monkey, II: cortical afferents. J Comp Neurol 1987; 262:271–289
51. Vita A, Bressi S, Perani D, Invernizzi G, Giobbio GM, Dieci M, Garbarini M, Del Sole A, Fazio F: High-resolution SPECT study of regional cerebral blood flow in drug-free and drug-naive schizophrenic patients. Am J Psychiatry 1995; 152:876–882
52. Portas CM, Goldstein JM, Shenton ME, Hokama HH, Wible CG, Fischer I, Kikinis R, Donnino R, Jolesz FA, McCarley RW: Volumetric evaluation of the thalamus in schizophrenic male patients using magnetic resonance imaging. Biol Psychiatry 1998; 43:649–659
53. Saijo T, Abe T, Someya Y, Sassa T, Sudo Y, Suhara T, Shuno T, Asai K, Okubo Y: Ten year progressive ventricular enlargement in schizophrenia: an MRI morphometrical study. Psychiatry Clin Neurosci 2001; 55:41–47
54. Sokoloff P, Giros B, Martres MP, Bouthenet ML, Schwartz JC: Molecular cloning and characterization of a novel dopamine receptor (D3) as a target for neuroleptics. Nature 1990; 347:146–151
55. Landwehrmeyer B, Mengod G, Palacios JM: Dopamine D3 receptor mRNA and binding sites in human brain. Brain Res Mol Brain Res 1993; 18:187–192
56. Murray AM, Ryoo HL, Gurevich E, Joyce JN: Localization of dopamine D3 receptors to mesolimbic and D2 receptors to mesostriatal regions of human forebrain. Proc Natl Acad Sci USA 1994; 91:11271–11275
57. Welham J, Stedman T, Clair A: Choosing negative symptom instruments: issues of representation and redundancy. Psychiatry Res 1999; 87:47–56

International Journal of Neuropsychopharmacology (2005), 8, 143–144. Copyright © 2004 CINP
DOI: 10.1017/S1461145704004961

The necessary parameters for estimating the time-course of receptor occupancy

Received 3 November 2004; Reviewed 16 November 2004; Revised 19 November 2004; Accepted 28 November 2004

The dissociation of the kinetics between plasma and the brain has been reported for antipsychotic drugs such as risperidone and olanzapine (Tauscher et al., 2002), and the kinetic profile of antipsychotics at receptor sites has been viewed as an important profile for antipsychotic actions and dosing schedule (Tauscher et al., 2002). Our recent report in this Journal (Takano et al., 2004) showed that the time-course of receptor occupancy could be estimated using plasma pharmacokinetics and drug-affinity parameters.

Tort et al. (2005) and Olsson and Farde (2005) presented interesting views based on our report (Takano et al., 2004), but there seem to be some misunderstandings. Tort et al. used equation (2) in their letter and simulated a curve that is different from the curve simulated using equation (2): $C = me^{-bt}$ in our report. Importantly, 'm' in equation (2) is a value derived from the measured plasma concentration data, whereas Tort et al. seem to assume that 'm' in our equation (2) is related to the ED_{50} value, which is a parameter for in-vivo affinity. However, ED_{50} is independent of the plasma concentration parameter m.

Tort et al. (2005) and Olsson and Farde (2005) pointed out that the value for 'the half-life of receptor occupancy' is dependent on the initial receptor occupancy (O_0) and not on the affinity of the drug. Although we used 'the half-life of receptor occupancy' as an index for the time-course of receptor occupancy, the proposed concept of half-life is not the same as that used for the plasma concentration. As we mentioned in our report, the time- course of receptor occupancy is not an exponential or linear function (Takano et al., 2004). The index 'the half-life of the receptor occupancy' is dependent on the initial occupancy value, but it needs to be pointed out that the initial occupancy value itself is a derivative of the ED_{50} value as can be seen from equation (3) in our report: $D_{2,occu} = 100 \times me^{-bt}/(ED_{50} + me^{-bt})$ (Takano et al., 2004)

$$O_0 = 100 \times m/(ED_{50} + m), \quad (4)$$

where O_0 is the receptor occupancy at time 0, which was defined as the initial occupancy by Olsson and Farde (2005).

As seen from equation (3), the time-course of receptor occupancy is determined by four parameters (ED_{50}, m, b and t). As suggested in our simulation study, the half-life of receptor occupancy ($R_oT_{\frac{1}{2}}$) can be operationally defined as the time required to reach half of the initial receptor occupancy value. From equation (3), the half-life of receptor occupancy ($R_oT_{\frac{1}{2}}$) can be expressed as follows:

$$R_oT_{\frac{1}{2}} = -\frac{1}{b} \times \ln(1/(m/ED_{50} + 1)), \quad (5)$$

From equation (5), three parameters (ED_{50}, m and b), namely, in-vivo affinity and plasma-concentration data, are keys in calculations of the half-life of receptor occupancy. Using equation (4), equation (5) can also be expressed as

$$R_oT_{\frac{1}{2}} = -\frac{1}{b} \times \ln((100 - O_0)/(200 - O_0)). \quad (6)$$

Although our definition [equation (5)] and the definition of Olsson and Farde (2005) [equation (6)] look different, these two definitions are essentially the same.

In conclusion, the time-course of receptor occupancy as described using initial occupancy and the magnitude of change (see Figure 3 in Takano et al., 2004) is dependent on in-vivo affinity, plasma-concentration kinetics and time (ED_{50}, m, b and t). The time-course of receptor occupancy is a consequence of a complex series of conditions. The suggested index 'half-life of receptor occupancy' is one aspect of the concept. It is the entire time-course of receptor occupancy that serves as the fundamental data in investigations of drug dynamics in the brain.

Acknowledgements

This work was supported by the Neuroscience Project of the National Institute of Radiological Sciences, Chiba, Japan.

Statement of Interest

None.

Address for correspondence: Dr A. Takano, Brain Imaging Project, National Institute of Radiological Sciences, Chiba, Japan. 9-1, 4-Chome, Anagawa, Inage-ku, Chiba-shi, Japan 263-8555.
Tel.: +81-43-206-3194 *Fax*: +81-43-253-0396
E-mail: aktakano@nirs.go.jp

References

Olsson H, Farde L (2005). Half-life of receptor occupancy – a meaningless concept. *International Journal of Neuropsychopharmacology 8*, 141–142. DOI: 10.1017/S1461145704004766.

Takano A, Suhara T, Ikoma Y, Yasuno F, Maeda J, Ichimiya T, Sudo Y, Inoue M, Okubo Y (2004). Estimation of the time-course of dopamine D_2 receptor occupancy in living human brain from plasma pharmacokinetics of antipsychotics. *International Journal of Neuropsychopharmacology 7*, 19–26.

Tauscher J, Jones C, Remington G, Zipursky RB, Kapur S (2002). Significant dissociation of brain and plasma kinetics with antipsychotics. *Molecular Psychiatry 7*, 317–321.

Tort A, Souza D, Lara D (2005). On the simulation of the time-course of dopamine D2 receptor occupancy from the pharmacokinetics of antipsychotics. *International Journal of Neuropsychopharmacology 8*, 137–139. DOI: 10.1017/S1461145704004778.

Akihiro Takano, Tetsuya Suhara
Brain Imaging Project, National Institute of Radiological Sciences, Chiba, Japan

Psychiatry and Clinical Neurosciences (2004), **58**, 330–332

Short Communication

Relation between cortical dopamine D_2 receptor occupancy and suppression of conditioned avoidance response in non-human primate

AKIHIRO TAKANO, MD, PhD,[1,2] TETSUYA SUHARA, MD, PhD,[1,2] JUN MAEDA,[1,2] KIYOSHI ANDO, PhD,[1,2,3] TAKASHI OKAUCHI, MSc,[1,2] SHIGERU OBAYASHI, MD, PhD,[1,2] TAKASHI NAKAYAMA, MD, PhD[1,2] AND SHITIJ KAPUR, MD, PhD[4]

[1]*Brain Imaging Project, National Institute of Radiological Sciences, Chiba,* [2]*CREST, Japan Science and Technology Corporation (JST), Kawaguchi,* [3]*Central Laboratories for Experimental Animals, Kawasaki, Japan and* [4]*Center for Addiction and Mental Health, Toronto, Ontario, Canada*

Abstract Suppression of the conditioned avoidance response (CAR), a useful test for screening for antipsychotic effects, has been discussed in relation to the blockade of dopaminergic transmission. The purpose of the present paper was to investigate the relationship between cortical dopamine D_2 receptor occupancy and the suppression of CAR by haloperidol in non-human primate. The avoidance rate was measured for four different doses of haloperidol treatment in a rhesus monkey, and the cortical D_2 receptor occupancy was measured in a parallel session using positron emission tomography with [^{11}C]FLB 457. The successful avoidance response rate was decreased for doses of 10 and 30 μg/kg of haloperidol, and this decrement was associated with 65–77% of D_2 receptor occupancy. It is suggested that the threshold level of cortical dopamine D_2 receptor occupancy for the suppression of CAR is demonstrated in the present study.

Key words [^{11}C]FLB 457, conditioned avoidance response, dopamine D_2 receptor occupancy, positron emission tomography.

INTRODUCTION

The conditioned avoidance response (CAR) has been regarded as a reliable tool for screening compounds for antipsychotic properties.[1] Most antipsychotic drugs induce high levels of striatal and extrastriatal (cortical) dopamine D_2 receptor occupancy at clinical doses, as measured by positron emission tomography (PET).[2,3] The suppression of CAR by antipsychotic drugs has been discussed in relation to the dopamine-blocking properties of antipsychotics, but most of the evidence was indirect.[4] A recent report by Wadenberg *et al.* showed a relationship between the suppression of CAR and striatal dopamine D_2 receptor occupancy in the rodent, indicating that striatal D_2 receptor occupancy of approximately 70–75% by haloperidol reliably elicited suppression of CAR avoidance.[5] Extrastriatal dopamine D_2 receptor occupancy can be measured in humans as well as in awake rhesus monkeys using [^{11}C]FLB 457.[3,6]

The purpose of the present paper was to investigate the relationship between dopamine D_2 receptor occupancy in the cortex, which is suggested to contain important sites of antipsychotic drug action,[7,8] and the suppression of CAR using a within-subject design and parallel measurements of occupancy and CAR in the same awake non-human primate.

METHODS

One male rhesus monkey (6.5 kg) was used in the present experiment. The present study was approved by the Animal Ethics Committee of the National Institute of Radiological Sciences, Chiba, Japan. The monkey was maintained and handled in accordance with

Correspondence address: Dr Tetsuya Suhara, Brain Imaging Project, National Institute of Radiological Sciences, 4-9-1, Anagawa, Inage-ku, Chiba 263-8555, Japan. Email: suhara@nirs.go.jp

Received 12 August 2003; revised 6 November 2003; accepted 16 November 2003.

the Guidelines for Animal Experimentation at the National Institute of Radiological Sciences, Japan. The monkey was trained for the lever-press CAR task on a monkey chair in an upright position. A light stimulus (conditioned stimulus: CS) for 5 s and then an electric shock to the tail of the monkey (2 mA) (unconditioned stimulus: US) for 2 s were presented using a specially designed controller (Ohara Ika Sangyo, Tokyo, Japan). The monkey was required to press the lever to avoid the shock. One trial consisted of a pair of CS and US with an intertrial interval (ITI) of 3 s. One session consisted of 20 trials. The monkey was considered to have reached a level of having learned the criteria after it showed a stable avoidance rate of 85% for 3 consecutive days. Saline or 1, 3, 10 or 30 μg/kg of haloperidol was administered intravenously, and each session of CAR was conducted at 20, 60, 120, 240 and 480 min after the administration. One session of CAR was performed 30 min before the drug administration to confirm that the avoidance rate exceeded 85%.

All PET acquisitions were performed in the awake state, separated from the CAR task for technical reasons, that is, the location of the white light on the steel plate was difficult to see from inside the PET gantry. After a transmission scan of 1 h for attenuation correction, a bolus of [^{11}C]FLB 457 (89.7 ± 11.6 MBq) with high specific radioactivity (117.4 ± 10.0 GBq/mmol) was injected intravenously. Dynamic scans were performed for 120 min with a specially designed animal PET scanner (SHR-7700, Hamamatsu Photonics, Hamamatsu, Japan). The first PET scan was performed as a baseline before CAR training. Based on the previous report that maximal behavioral effects were observed 20–90 min after subcutaneous injection to rats,[5] the PET scans with drug were performed 60 min after the injection of 1, 3, 10 or 30 μg/kg of haloperidol. Regions of interest (ROI) were placed on the prefrontal cortex, temporal cortex and cerebellum with reference to the individual MR images and a monkey brain atlas. The binding of [^{11}C]FLB 457 was quantified using a three-parameter simplified reference tissue model.[9] The cerebellum was used as reference tissue because it is nearly devoid of dopamine D_2 receptors.[10] The occupancy of dopamine D_2 receptors was estimated using the following equation: $Occ = (BP_{free} - BP_{drug}) \times 100 / BP_{free}$, where Occ is the percentage occupancy, BP_{free} is the binding potential of the monkey in a drug-free state, and BP_{drug} is the binding potential of the monkey with haloperidol.

RESULTS

It took 1 month for the monkey to reach the qualifying criteria for CAR. The CAR rate after saline administration was 90–100%. The CAR rate was not significantly affected by 1 or 3 μg/kg of haloperidol, but it was significantly decreased after 10 or 30 μg/kg of haloperidol. The mean cortical dopamine D_2 receptor occupancies were 44.7 ± 4.5% with 1 μg/kg and 52.0 ± 5.9% with 3 μg/kg (Table 1). With 10 μg/kg of haloperidol, the avoidance rate decreased to 75% at 20 min, 25% at 60 min, 10% at 120 min and 240 min, and 0% at 480 min. With 30 μg/kg of haloperidol, the avoidance rate decreased to 5% at 20 min, 10% at 60 min and 5% at 120 min, and it was 0% at 240 min and 480 min. The mean cortical dopamine D_2 receptor occupancies were 65.6 ± 0.6% with 10 μg/kg of haloperidol and 76.5 ± 0.0% with 30 μg/kg (Table 1).

Table 1. Relationship between dopamine D_2 receptor occupancy and CAR rate

Haloperidol injected dose (μg/kg)	Dopamine D_2 receptor occupancy (%) Prefrontal cortex	Temporal cortex	CAR rate (%)
0	–	–	90
1	47.8	41.5	100
3	56.1	47.8	100
10	65.1	66.0	25
30	76.5	76.5	10

CAR rate, percentage of conditioned avoidance response at 60 min after injection of haloperidol.

DISCUSSION

The present results demonstrate a threshold-like relationship between the degree of cortical dopamine D_2 receptor occupancy and the suppression of CAR when measured in parallel in an awake CAR-trained monkey. These results were consistent with the rat experiment of CAR in that 70–75% of striatal dopamine D_2 receptor occupancy was measured with the suppression of CAR.[5] It has been reported that 65–70% of striatal D_2 receptor occupancy is necessary to induce sufficient antipsychotic effects in a clinical setting.[3,11,12] Similar claims have also been made for extrastriatal dopamine D_2 occupancy.[13]

Although the mechanism of the CAR task is not fully understood, it has been suggested that mesocorticolimbic dopamine pathways are involved in the CAR response,[14] and increased extracellular dopamine in the prefrontal cortex was reported during the acquisition of avoidance response.[15] The avoidance response can be impaired by damage in the limbic–cortical region, such as in the medial prefrontal cortex and amygdala.[16,17]

Although our results are consistent with the notion of extrastriatal dopamine transmission being important for CAR, they are subject to several caveats. We did not measure the striatal D_2 occupancy. In some previous work the striatal and extrastriatal D_2 occupancies were correlated in human studies.[13] One cannot be sure that striatal dopamine D_2 blockade does not perhaps make a contribution to this effect.

And although we observed a clear relationship between D_2 occupancy and outcome at the 1 h mark, the suppression of CAR by 10 and 30 μg/kg of haloperidol lasted for 8 h after the administration. This can be explained by the results from a human study, in which sustained high D_2 receptor occupancy was observed with a clinical dose of haloperidol,[18] suggesting that the optimal time for measurement of the occupancy with haloperidol might be later than that of the present study.

The effects of haloperidol on the noticeptive thresholds might be an important factor in the paradigm of CAR. However, these effects were reported to appear at larger doses than the ones used in the present study (1–30 μg/kg).[19]

In conclusion, the present preliminary results demonstrated a threshold in cortical dopamine D_2 receptor occupancy for the suppression of monkey CAR by haloperidol. The combination of behavioral studies of awake non-human primates with parallel neurochemical measurements can be a useful tool for investigating the mechanism of action of antipsychotic drugs.

REFERENCES

1. Wadenberg ML, Hicks PB. The conditioned avoidance response test re-evaluated: is it a sensitive test for the detection of potentially atypical antipsychotics? *Neurosci. Biobehav. Rev.* 1999; **23**: 851–862.
2. Farde L, Nordström AL, Wiesel FA, Pauli S, Halldin C, Sedvall G. Positron emission tomographic analysis of central D_1 and D_2 dopamine receptor occupancy in patients treated with classical neuroleptics and clozapine. Relation to extrapyramidal side effects. *Arch. Gen. Psychiatry* 1992; **49**: 538–544.
3. Farde L, Suhara T, Nyberg S *et al.* A PET-study of [^{11}C]FLB 457 binding to extrastriatal D_2-dopamine receptors in healthy subjects and antipsychotic drug treated patients. *Psychopharmacology* 1997; **133**: 396–404.
4. Davies JA, Jackson B, Redfern PH. The effect of anti-Parkinsonian drugs on haloperidol-induced inhibition of the conditioned-avoidance response in rats. *Neuropharmacology* 1973; **12**: 735–740.
5. Wadenberg ML, Soliman A, VanderSpek SC, Kapur S. Dopamine D_2 receptor occupancy is a common mechanism underlying animal models of antipsychotics and their clinical effects. *Neuropsychopharmacology* 2001; **25**: 633–641.
6. Okauchi T, Suhara T, Maeda J, Kawabe K, Obayashi S, Suzuki K. Effect of endogenous dopamine on extrastriated [^{11}C]FLB 457 binding measured by PET. *Synapse* 2001; **41**: 87–95.
7. Pilowsky LS, Mulligan RS, Acton PD, Ell PJ, Costa DC, Kerwin RW. Limbic selectivity of clozapine. *Lancet* 1997; **350**: 490–491.
8. Lidow MS, Williams GV, Goldman-Rakic PS. The cerebral cortex: a case for a common site of action of antipsychotics. *Trends Pharmacol. Sci.* 1998; **19**: 136–140.
9. Lammertsma AA. Simplified reference tissue model for PET receptor studies. *Neuroimage* 1996; **4**: 153–158.
10. Suhara T, Sudo Y, Okauchi T *et al.* Extrastriatal dopamine D_2 receptor density and affinity in the human brain measured by 3D PET. *Int. J. Neuropsychopharmcol.* 1999; **2**: 73–82.
11. Nordström AL, Farde L, Wiesel FA *et al.* Central D_2-dopamine receptor occupancy in relation to antipsychotic drug effects: a double-blind PET study of schizophrenic patients. *Biol. Psychiatry* 1993; **33**: 227–235.
12. Kapur S, Zipursky R, Jones C, Remington G, Houle S. Relationship between dopamine D_2 occupancy, clinical response, and side effects: a double-blind PET study of first-episode schizophrenia. *Am. J. Psychiatry* 2000; **157**: 514–520.
13. Talvik M, Nordström AL, Nyberg S, Olsson H, Halldin C, Farde L. No support for regional selectivity in clozapine-treated patients: a PET study with [^{11}C]raclopride and [^{11}C]FLB 457. *Am. J. Psychiatry* 2001; **158**: 926–930.
14. Wadenberg ML, Ericson E, Magnusson O, Ahlenius S. Suppression of conditioned avoidance behavior by the local application of (-) sulpiride into the ventral, but not the dorsal, striatum of the rat. *Biol. Psychiatry* 1990; **28**: 297–307.
15. Stark H, Bischof A, Scheich H. Increase of extracellular dopamine in prefrontal cortex of gerbils during acquisition of the avoidance strategy in the shuttle-box. *Neurosci. Lett.* 1999; **264**: 77–80.
16. Jinks AL, McGregor IS. Modulation of anxiety-related behaviours following lesions of the prelimbic or infralimbic cortex in the rat. *Brain Res.* 1997; **772**: 181–190.
17. Roozendaal B, Koolhaas JM, Bohus B. The central amygdala is involved in conditioning but not in retention of active and passive shock avoidance in male rats. *Behav. Neural Biol.* 1993; **59**: 143–149.
18. Nordström AL, Farde L, Halldin C. Time course of D_2-dopamine receptor occupancy examined by PET after single oral doses of haloperidol. *Psychopharmacology* 1992; **106**: 433–438.
19. Main DC, Waterman AE, Kilpatrick IC. Behavioural analysis of changes in nociceptive thresholds produced by remoxipride in sheep and rats. *Eur. J. Pharmacol.* 1995; **287**: 221–231.

Development of a New Radioligand, *N*-(5-Fluoro-2-phenoxyphenyl)-*N*-(2-[^{18}F]fluoroethyl-5-methoxybenzyl)acetamide, for PET Imaging of Peripheral Benzodiazepine Receptor in Primate Brain

Ming-Rong Zhang,*[†,§] Jun Maeda,[†,§] Masanao Ogawa,[†,§] Junko Noguchi,[†,§] Takehito Ito,[†,§] Yuichiro Yoshida,[†,§] Takashi Okauchi,[†,§] Shigeru Obayashi,[‡] Tetsuya Suhara,[‡] and Kazutoshi Suzuki[†]

Department of Medical Imaging, National Institute of Radiological Sciences, 4-9-1 Anagawa, Inage-ku, Chiba 263-8555, Japan; Brain Imaging Project, National Institute of Radiological Sciences, 4-9-1 Anagawa, Inage-ku, Chiba 263-8555, Japan; and SHI Accelerator Service Co. Ltd., 5-9-11 Kitashinagawa, Shinagawa-ku, Tokyo 141-8686, Japan

Received October 1, 2003

To develop a positron emission tomography (PET) ligand for imaging the 'peripheral benzodiazepine receptor' (PBR) in brain and elucidating the relationship between PBR and brain diseases, four analogues (**4**–**7**) of *N*-(2,5-dimethoxybenzyl)-*N*-(5-fluoro-2-phenoxyphenyl)-acetamide (**2**) were synthesized and evaluated as ligands for PBR. Of these compounds, fluoromethyl (**4**) and fluoroethyl (**5**) analogues had similar or higher affinities for PBR than the parent compound **2** (K_i = 0.16 nM for PBR in rat brain sections). Iodomethyl analogue **6** displayed a moderate affinity, whereas tosyloxyethyl analogue **7** had weak affinity. Radiolabeling was performed for the fluoroalkyl analogues **4** and **5** using fluorine-18 (^{18}F, β^+; 96.7%, $T_{1/2}$ = 109.8 min). Ligands [^{18}F]**4** and [^{18}F]**5** were respectively synthesized by the alkylation of desmethyl precursor **3** with [^{18}F]fluoromethyl iodide ([^{18}F]**8**) and 2-[^{18}F]fluoroethyl bromide ([^{18}F]**9**). The distribution patterns of [^{18}F]**4** and [^{18}F]**5** in mice were consistent with the known distribution of PBR. However, compared with [^{18}F]**5**, [^{18}F]**4** displayed a high uptake in the bone of mice. The PET image of [^{18}F]**4** for monkey brain also showed significant radioactivity in the bone, suggesting that this ligand was unstable for in vivo defluorination and was not a useful PET ligand. Ligand [^{18}F]**5** displayed a high uptake in monkey brain especially in the occipital cortex, a region with richer PBR than the other regions in the brain. The radioactivity level of [^{18}F]**5** in monkey brain was 1.5 times higher than that of [^{11}C]**2**, and 6 times higher than that of (*R*)-(1-(2-chlorophenyl)-*N*-[^{11}C]methyl,*N*-(1-methylpropyl)isoquinoline ([^{11}C]**1**). Moreover, the in vivo binding of [^{18}F]**5** was significantly inhibited by PBR-selective **2** or **1**, indicating that the binding of [^{18}F]**5** in the monkey brain was mainly due to PBR. Metabolite analysis revealed that [^{18}F]**4** was rapidly metabolized by defluorination to [^{18}F]F$^-$ in the plasma and brain of mice, whereas [^{18}F]**5** was metabolized by debenzylation to a polar product [^{18}F]**13** only in the plasma. No radioactive metabolite of [^{18}F]**5** was detected in the mouse brain. The biological data indicate that [^{18}F]**5** is a useful PET ligand for PBR and is currently used for imaging PBR in human brain.

Introduction

'Peripheral benzodiazepine receptor' (PBR), which was initially identified in the peripheral tissues, is located on the mitochondrial outer membrane in several organs including the kidney, nasal epithelium, lung, heart, and endocrine organs such as the adrenal, testis, and pituitary gland.[1–3] Later studies further demonstrated the presence of PBR in the central nervous system.[4–6] The PBR density in the brain was increased in injured brain, and this increase has been used as an indicator of neuronal damage[7] and several neurodenerative disorders, such as Alzheimer's disease,[8] Huntington's disease,[9] Wernicke's encephalopathy,[10] multiple sclerosis,[11] and stroke.[12] In addition, a relationship between alterations of PBR and epileptic foci have been proposed.[13,14] These findings have resulted in the development of a radioligand labeled by a positron-emitter, which has made possible to visualize the distribution of PBR in the brain.[15–19]

Scheme 1. Chemical Structures of [^{11}C]**1** and [^{11}C]**2** Analogues

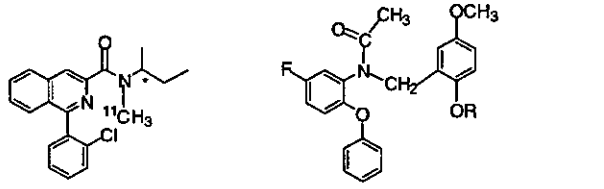

[^{11}C](*R*)-PK 11195 ([^{11}C]**1**)

DAA1106 (**2**): R = CH_3
[^{11}C]DAA1106 ([^{11}C]**2**): R = $^{11}CH_3$
DAA1123 (**3**): R = H
[^{18}F]FMDAA1106 ([^{18}F]**4**): R = $^{18}FCH_2$
[^{18}F]FEDAA1106 ([^{18}F]**5**): R = $^{18}FCH_2CH_2$

(*R*)-(1-(2-Chlorophenyl)-*N*-[^{11}C]methyl,*N*-(1-methylpropyl)isoquinoline ([^{11}C](*R*)-PK 11195, [^{11}C]**1**, Scheme 1) is a clinically useful positron emission tomography (PET) ligand for imaging PBR in cases of several brain

* Corresponding author: Tel: 81-43-206-4041; Fax: 81-43-206-3261; E-mail: zhang@nirs.go.jp.
† Department of Medical Imaging, National Institute of Radiological Sciences.
‡ Brain Imaging Project, National Institute of Radiological Sciences.
§ SHI Accelerator Service Co. Ltd.

10.1021/jm0304919 CCC: $27.50
Published on Web 03/26/2004

diseases.[20-23] However, the signal of [^{11}C]**1** in the primate brain was not high enough for quantitative analysis using PET because of its low uptake into the brain.[23] Therefore, the precise characterization of PBR in primate brain awaits development of new PET ligands with improvements over [^{11}C]**1**. In 1998, *N*-(2,5-dimethoxybenzyl)-*N*-(5-fluoro-2-phenoxyphenyl)acetamide (DAA1106, **2**, Scheme 1) was reported as a potent and selective ligand for PBR by the Taisho Pharmaceutical's group.[24-27] Compound **2** had a high affinity for PBR in mitochondrial fractions of rat (K_i = 0.043 nM) and monkey (K_i = 0.188 nM) brains.[25] Moreover, **2** had weak or negligible affinities (IC_{50} > 10 μM) for other receptors, ion channels, uptake/transporters, and second messengers.[26] Thus, we previously synthesized [^{11}C]**2**[28] as a PET ligand for PBR by reacting the desmethyl precursor *N*-(5-fluoro-2-phenoxyphenyl)-*N*-(2-hydroxy-5-methoxybenzyl)acetamide[24,27] (DAA1123, **3**) with [^{11}C]-CH_3I. The in vitro and in vivo evaluation using mouse, rat and monkey demonstrated that [^{11}C]**2** had high specific binding with PBR in the brains and about a 4-fold higher uptake of radioactivity in the monkey brain than [^{11}C]**1**.[28,29] Now, [^{11}C]**2** is being used to investigate PBR in the human brain in our facility.

In general, the short half-life of a ^{11}C labeled ligand (β^+; 99.8%, $T_{1/2}$ = 20.4 min) often limits its usefulness if a dynamic PET experiment has a turnover time longer than 100 min. Since ^{18}F has advantages over ^{11}C, with a longer half-life (110 min vs. 20 min) and a lower positron energy (650 keV vs 960 keV), an ^{18}F-labeled ligand gives higher quality images with a higher spatial resolution in PET measurements. Moreover, ^{18}F is convenient for long-time storage and long-distance transportation to other facilities. To develop ^{18}F-labeled PET ligand with improved properties compared to [^{11}C]**2**, we previously prepared two [^{18}F]fluoroalkyl analogues of **2**: *N*-(5-fluoro-2-phenoxyphenyl)-*N*-(2-[^{18}F]fluoromethyl-5-methoxybenzyl)acetamide ([^{18}F]FM-DAA1106, [^{18}F]**4**) and *N*-(5-fluoro-2-phenoxyphenyl)-*N*-(2-[^{18}F]fluoroethyl-5-methoxybenzyl)acetamide ([^{18}F]-FEDAA1106, [^{18}F]**5**) as putative radioligands for PBR (Scheme 1).[30] Preliminary studies revealed that analogues **4** and **5** have similar or higher inhibitory activity (IC_{50}) for PBR in the rat brain than **2**.[30] The ex vivo autoradiograms of [^{18}F]**4** and [^{18}F]**5** binding sites in rat brain revealed significantly high radioactivity in the olfactory bulb and cerebellum, the richer regions of PBR compared with other brain regions.[30]

In this study, we synthesized four analogues (**4**–**7**, Scheme 2) including two novel compounds: (*N*-(5-fluoro-2-phenoxyphenyl)-*N*-(2-iodomethyl-5-methoxybenzyl)acetamide (**6**) and *N*-(5-fluoro-2-phenoxyphenyl)-*N*-(5-methoxy-2-tosyloxyethylbenzyl)acetamide (**7**). Using autoradiography technique, we measured the binding affinities (K_i) of **4**–**7** to PBR and the central benzodiazepine receptor (CBR). We labeled the fluoroalkyl analogues **4** and **5** using ^{18}F and prepared the radioactive products in reproducible radiochemical yields. We examined the regional distribution of [^{18}F]**4** and [^{18}F]**5** in mice and measured the percentages of unmetabolized [^{18}F]**4** and [^{18}F]**5** in the plasma and brain. Using PET, we determined the uptake of [^{18}F]**4** and [^{18}F]**5** and elucidated the specific binding of [^{18}F]**5** to PBR in the monkey brain.

Scheme 2. Chemical Synthesis of Compounds **4**–**7**[a]

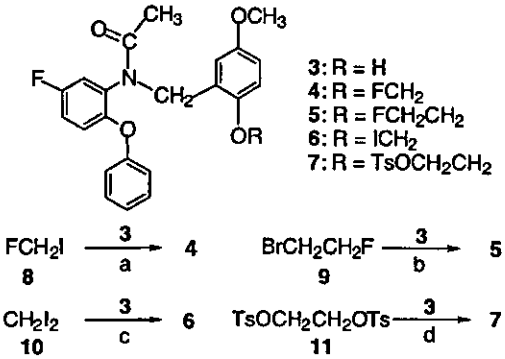

[a] Reagents and conditions: (a) NaH, DMF, 0 °C, 5 h, 79%; (b) NaH, DMF, 80 °C, 8 h, 65%; (c) NaH, DMF, 25 °C, 3 h, 34%; (d) NaH, DMF, 0 °C, 5 h, 46%.

Scheme 3. Radiosynthesis of [^{18}F]**4** and [^{18}F]**5** by Two Methods[a]

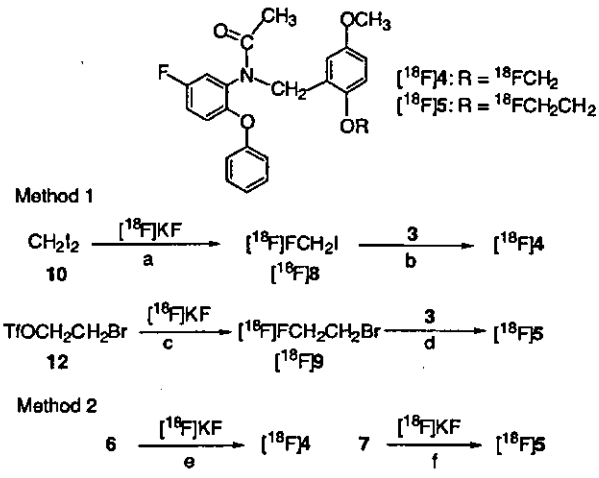

[a] Reagents and conditions: (a) 110 °C, 10 min, 8%; (b) NaH, DMF, −15 °C, 3 min, 90%; (c) *o*-dichlorobenzene, 130 °C, 5 min, 55%; (d) NaH, DMF, −15 °C, 10 min and then 120 °C, 10 min, 82%; (e) DMF, 30–120 °C, 1–15 min, 2–37%; (f) DMF, 30–120 °C, 1–15 min, 2–60%.

Results and Discussion

Chemistry. The four analogues **4**–**7** were synthesized according to the reaction sequences lineated in Scheme 2. Reaction of the desmethyl precursor **3**[24,27] with excess fluoromethyl iodide[31] (FCH_2I, **8**) in the presence of NaH at 0 °C for 5 h gave the fluoromethyl analogue **4**. Treatment of **3** with 2-fluoroethyl bromide (FCH_2CH_2Br, **9**) and NaH at 80 °C gave the fluoroethyl analogue **5**. The iodomethyl analogue **6** was prepared by the reaction of **3** with diiodomethane (CH_2I_2, **10**) and NaH at 25 °C for 3 h. The tosyloxyethyl analogue **7** was obtained by treating **3** with excess ethylene ditosylate (**11**) and NaH at 0 °C.

Radiosynthesis. Ligands [^{18}F]**4** and [^{18}F]**5** were prepared by two methods according to Scheme 3. The first method was a two-step reaction sequence which involved the preparation of the radioactive intermediate [^{18}F]fluoromethyl iodide ([^{18}F]FCH_2I, [^{18}F]**8**) or 2-[^{18}F]fluoroethyl bromide ([^{18}F]FCH_2CH_2Br, [^{18}F]**9**), followed by the alkylation of **3** with [^{18}F]**8** or [^{18}F]**9**. The second method was direct nucleophilic replacement of the iodomethyl analogue **6** or tosyloxyethyl analogue **7**

with $[^{18}F]F^-$. As for the two-step method, the alkylating intermediate [^{18}F]**8** or [^{18}F]**9** was prepared by the reaction of $[^{18}F]F^-$ with **10** or 2-trifluoromethanesulfonyloxyethyl bromide ($BrCH_2CH_2OTf$, **12**) by using a newly developed automated system.[32,33] After the fluorine reaction finished, [^{18}F]**8** or [^{18}F]**9** was purified by distillation and directly trapped in a solution of DMF containing **3** and NaH at −15 °C. The purification of [^{18}F]**8** (bp: 53−54 °C) or [^{18}F]**9** (bp: 71.5 °C) by distillation was effective, because this procedure can leave behind all nonvolatile impurities such as metal ions from the cyclotron target, the unreacted $[^{18}F]F^-$, and the phase-transfer reagent Kryptofix 222/K_2CO_3. After the radioactive [^{18}F]**8** or [^{18}F]**9** trapping ended, the [^{18}F]fluoromethylation finished perfectly, while the [^{18}F]fluoroethylation required a further 10 min at 120 °C. As for the direct method, heating **6** and **7** with $[^{18}F]F^-$ at 30−120 °C gave [^{18}F]**4** and [^{18}F]**5**. However, the radiochemical yields were not reproducible (2%−60%), and purifying [^{18}F]**4** and [^{18}F]**5** from the reaction mixtures was often difficult since the many impurities resulting from the target and reaction greatly reduced the efficiency. After comparing the reaction conditions and radiochemical yields, we synthesized [^{18}F]**4** and [^{18}F]**5** by the two-step reaction method (Method 1) via the intermediates [^{18}F]**8** and [^{18}F]**9**, respectively.

Reversed phase semipreparative HPLC purification of the reaction mixtures gave [^{18}F]**4** and [^{18}F]**5** in 45 ± 10% (n = 4) and 12 ± 4% (n = 4) radiochemical yields based on $[^{18}F]F^-$, corrected for the physical decay in a synthesis time of 63 ± 4 min and 50 ± 3 min. The identity of the desired product was confirmed by coinjection with the corresponding nonradioactive **4** or **5** on reverse phase analytic HPLC. In the final product solutions, the radiochemical purity of [^{18}F]**4** or [^{18}F]**5** was higher than 98% and the specific activity was 40−65 GBq/μmol for [^{18}F]**4** and 110−145 GBq/μmol for [^{18}F]**5** as determined from the mass measured by HPLC/UV analysis. No significant peak corresponding to **3** was observed in the HPLC for the final products. Moreover, the radiochemical purities of [^{18}F]**4** and [^{18}F]**5** remained >95% after 180 min at 25 °C, and they were stable as PET ligands while performing the evaluation.

In Vitro Binding Assays. The in vitro binding affinities (K_i) of the four analogues **4**−**7** for PBR were determined from competition for the [^{11}C]**2** binding to PBR using quantitative autoradiography of rat brain sections[34,35] (Table 1). Among these compounds, the fluoroethyl analogue **5** was the most active toward PBR. The K_i value (0.078 nM) of **5** was 2-fold higher than that of **2**, and 10-fold higher than that of **1**. This result suggested that substituting the OCH_3 group with OCH_2CH_2F group was favorable for augmenting its binding affinity for PBR. The fluoromethyl analogue **4** displayed a similar affinity to **2**, suggesting that substitution with a OCH_2F group did not obviously affect the affinity. This may be due to the molecular similarity and bioisoteric property of the OCH_2F and OCH_3 groups. The iodomethyl analogue **6** had 30 times lower affinity than **2**, while the tosyloxyethyl analogue **7** was 110 times weaker than **2**. These results suggested that the relative bulk groups in this series were not favorable for the binding of PBR. However, although it was moderately potent (K_i = 4.8 nM) for PBR, the iodomethyl analogue **6** may become a suitable candidate of a SPECT ligand for imaging PBR. Similarly, the binding affinities of **4**−**7** for CBR were measured using CBR-selective [^{11}C]flumazenil. As shown in Table 1, **4**−**7** did not display significant inhibitory effects (K_i > 1 μM) on [^{11}C]flumazenil binding in the rat brain. The negligible affinities of these analogues for CBR may be due to a difference from the typical benzodiazepine structure, which resulted in high selectivity for PBR.

Table 1. In Vitro Binding Affinity (K_i) for PBR and CBR, and Octanol/Phosphate Buffer Distribution Coefficient (log D)

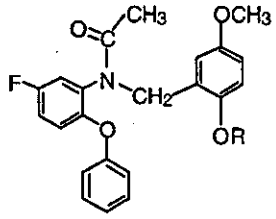

		K_i(nM)[a]		
ligand	R	PBR[b]	CBR[c]	log D[d]
4	FCH_2	0.17 ± 0.02	>1000	3.70
5	FCH_2CH_2	0.078 ± 0.01	>1000	3.81
6	ICH_2	4.8 ± 0.68	>1000	4.02
7	$TsOCH_2CH_2$	18.1 ± 1.30	>1000	4.65
2	CH_3	0.16 ± 0.02	>1000	3.65
1		0.83 ± 0.24	>1000	2.78

[a] Values represent the mean obtained from 9 concentrations of compound using at least 8 slices of rat brain (n = 3). [b] [^{11}C]**2** was incubated in the presence of the compounds examined. [c] [^{11}C]Flumazenil was incubated in the presence of the compounds examined. [d] The logD values were determined in the phosphate buffer (pH = 7.4)/octanol system using the shaking flask method. All results were presented as mean values (n = 3) with a maximum range of ±5%.

Biodistribution on Mice. The radioactivity distribution of [^{18}F]**4** and [^{18}F]**5** was measured in mice over 120 min (the data are shown in Supporting Information). These results revealed that [^{18}F]**4** and [^{18}F]**5** showed a similar distribution pattern of radioactivity in the regions examined except bone. As can be seen, high radioactivity levels (>5% ID/g) were found in tissues such as the lung, heart, kidney, and adrenal gland, organs known to be rich in PBR. The distribution patterns of uptake were in agreement with that of PBR in the peripheral system, which was consistent with the distribution of [^{11}C]**2** or [^{11}C]**1** in the mouse. The highest accumulations of [^{18}F]**4** and [^{18}F]**5** were found in the lung and these high levels were probably due to the high mitochondrial contents containing PBR in the organ. On the other hand, high radioactivities (2.6−4.4% ID/g for [^{18}F]**4** and 2.2−4.9% ID/g for [^{18}F]**5**) were also found in the brain, the target tissue in this experiment. The values were about 1.3−1.6-fold higher than that of [^{11}C]**2**, and 2−3-fold higher than that of [^{11}C]**1**, which was consistent with their higher partition coefficients as shown in Table 1. These findings suggested that [^{18}F]**4** and [^{18}F]**5** do pass across the brain−blood barrier (BBB), which is a prerequisite for a promising PET ligand.

In the bone of mouse, a significant difference in radioactivity was observed between [^{18}F]**4** and [^{18}F]**5**. The accumulation of [^{18}F]**5** in the bone was initially low and showed no increase from 30 min (0.31% dose/g) to 120 min (0.09% dose/g), which demonstrated the ex-

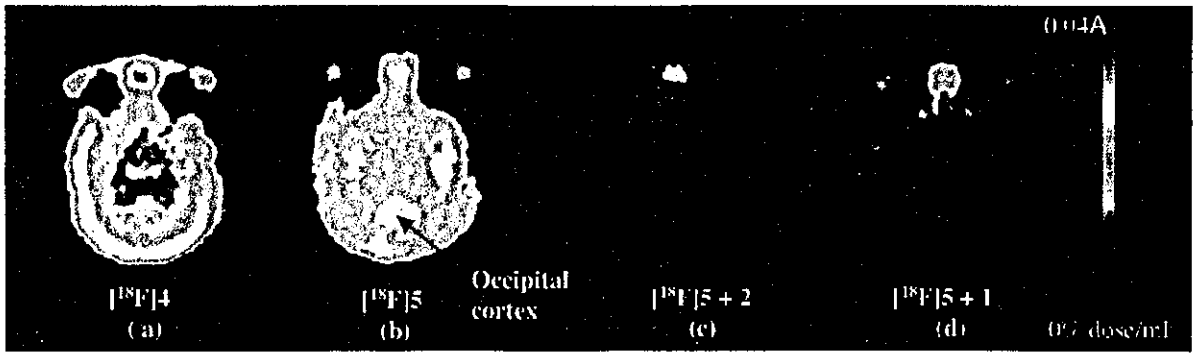

Figure 1. PET summation images of the monkey brain acquired between 30 and 180 min after [^{18}F]ligand injection. The images were obtained from the same subject. (a) [^{18}F]**4**; (b) [^{18}F]**5**; (c) [^{18}F]**5** after treatment with **2** (1 mg/kg); (d) [^{18}F]**5** after treatment with **1** (5 mg/kg). Significant radioactivity was observed in the bone after injection of [^{18}F]**4** (a). High radioactivity was observed in the occipital cortex after injection of [^{18}F]**5** (b), which was significantly inhibited by **2** (c) and **1** (d).

pected stability of the fluoroethyl group against in vivo defluorination. In contrast, after injection of [^{18}F]**4**, the radioactivity began to accumulate in the bone and reached 5.6% dose/g at 120 min, which was 50 times higher than that of [^{18}F]**5** in the bone. On consideration of the characteristic of [^{18}F]F^- to readily accumulate in bone, [^{18}F]**4** may be decomposed to [^{18}F]F^- by in vivo defluorination. Our previous findings also demonstrated that [^{18}F]fluoromethyl compounds are relatively unstable in comparison with the corresponding [^{18}F]fluoroethyl and [^{11}C]methyl compounds.[33] Therefore, [^{18}F]**4** may not be a useful PET ligand, even if it entered the brain and had some binding sites with PBR.

Monkey PET. The uptake of [^{18}F]**4** and [^{18}F]**5** in monkey brain was examined using PET. In the previous in vitro study for postmortem human brain, the highest density of PBR was observed in the occipital cortex,[36] so the region of interest (ROI) in this PET experiment was placed on the occipital cortex. Figure 1 shows typical PET summation images of the monkey brain acquired from 30 to 180 min after [^{18}F]**4** (a) and [^{18}F]**5** (b) injection (80–85 MBq/1.5 mL). The two images displayed a high accumulation of radioactivity in the brain especially in the occipital cortex. However, in comparison with [^{18}F]**5**, a marked accumulation of [^{18}F]**4** was observed in the bone. This image is visual evidence that [^{18}F]**4** was decomposed to [^{18}F]F^- in vivo as reflected in the high accumulation of [^{18}F]**4** in the mouse bone. Therefore, no further evaluation of [^{18}F]**4** was carried out using PET in monkey brain.

Figure 2 (circles) shows the time activity curve (TAC) of [^{18}F]**5** in the occipital cortex of monkey brain after intravenous (iv) injection. At 2 min after injection, a high level of radioactivity was observed in the occipital cortex, which then remained almost same level during PET measurement (180 min). The radioactivity of [^{18}F]**5** was 1.5 times higher than that of [^{11}C]**2**,[29] and 6 times higher than that of [^{11}C]**1**[29] at 30 min after injection. Pretreatment with nonradioactive **2** (1.0 mg/kg) gave a marked reduction of uptake for the image (Figure 1c) and TAC (Figure 2: triangles) of [^{18}F]**5** as compared to the control experiment which was obtained under the same conditions. As shown in Figure 2, pretreatment with **1** enhanced the initial maximal uptake of [^{18}F]**5**. The increase may be derived from [^{18}F]**5** dispossessed by mass nonradioactive **2** from lung abundant in PBR. Similar cases have been reported in the PET studies of

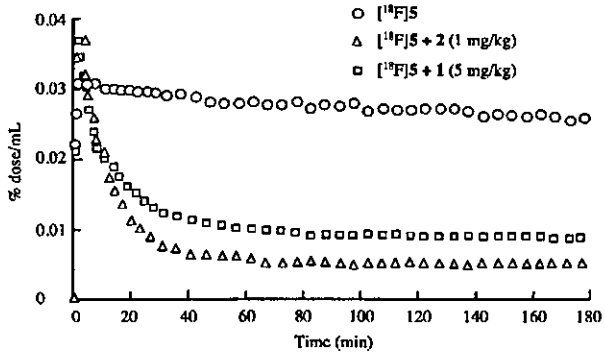

Figure 2. Time–activity curves (TACs) of [^{18}F]**5** in the occipital cortex of monkey brain. The radioactivity of the control (circles) was strongly inhibited by pretreatment with **2** (triangles) and **1** (squares).

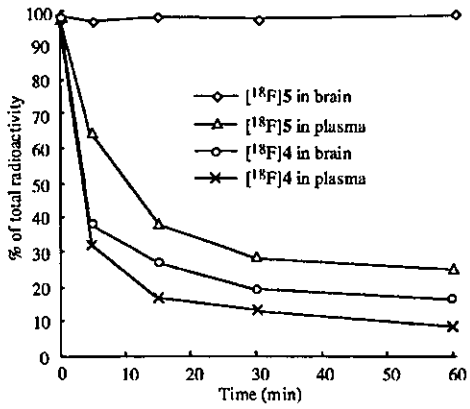

Figure 3. Percent conversion of [^{18}F]**4** or [^{18}F]**5** to metabolite in the mouse plasma and brain at several time points after iv injection of ligand (5–10 MBq) into the mice (n = 3). The unchanged tracers and metabolites were analyzed by HPLC for CH_3CN extracts from the plasma and brain homogenate prepared as described in the Experimental Section.

[^{11}C]**1**[36] and [^{11}C]**2**.[29] From 30 min after injection to the end (180 min) of the PET scan, pretreatment with **2** reduced the level of radioactivity to about 20% of the control. This result suggested high specific binding of [^{18}F]**5** present in the occipital cortex. Pretreatment with the PBR-selective **1** (5 mg/kg) also produced a significant reduction of radioactivity in the occipital cortex, as shown in the image (Figure 1d) and TAC (Figure 2: squares). The radioactivity was reduced to about 30%

Scheme 4. Metabolism of [^{18}F]**4** and [^{18}F]**5** in the Plasma and Brain

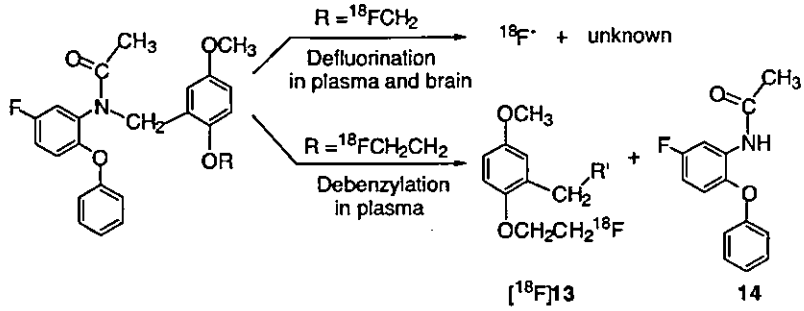

of the control from 30 min after injection to the end of the PET scan. The reduction percentage on the uptake of [^{18}F]**5** by **1** was slightly lower that by **2**, which was probably due to the weaker affinity of **1** for PBR and its lower penetration[27] into the brain than that of **2**. These findings confirmed that [^{18}F]**5** may have high specific binding for PBR in the monkey brain.

Metabolite Analysis. In the imaging brain study, the presence of metabolites in the plasma of the subject may preclude the evaluation of a PET ligand if the metabolites enter the brain and are retained/bound at the target sites. Therefore, metabolite analyses were performed for [^{18}F]**5** in the plasma and brain of mouse, and the plasma of monkey. For comparison, similar analyses were also performed for [^{18}F]**4**.

Figure 3 shows the percentages of unchanged [^{18}F]**4** and [^{18}F]**5** in the plasma and brain homogenate of mice measured by HPLC. After injection into the mouse, the fraction corresponding to the unmetabolized [^{18}F]**4** in the plasma or brain rapidly decreased to 32% or 35% at 5 min, and to 15% or 22% at 30 min. A major radioactive metabolite with high polarity was observed in the HPLC. Using ion exchange chromatography, the metabolite was assigned to [^{18}F]F$^-$. Since [^{18}F]F$^-$ is probably not brain permeable, [^{18}F]**4** may be metabolized in the plasma and brain, respectively (Scheme 4).

After its injection into the mouse, the amount of [^{18}F]**5** in the plasma continued to decrease during the entire experiment. The fraction corresponding to the unchanged [^{18}F]**5** in the plasma was 64% at 5 min, 29% at 30 min, and 25% of the total radioactivity at 60 min after injection. No [^{18}F]F$^-$ but another radioactive metabolite was observed in the HPLC. As estimated by its retention time (t_R = 1.9 min), the metabolite was much more polar than [^{18}F]**5** (t_R = 11.8 min). On the other hand, only [^{18}F]**5** was detected in the brain homogenate with no evidence (<5%) of any radioactive metabolites even at 60 min after injection.

The metabolite analysis was also performed using monkey plasma. After its injection into the monkey, [^{18}F]**5** in plasma decreased to 77% at 5 min, 56% at 30 min, and 18% at 90 min. From then, the amount of unchanged [^{18}F]**5** continued to decrease, while that of a radioactive metabolite increased to 90% by the end (180 min) of the PET experiment. The radioactive metabolite in the monkey plasma was the same metabolite determined in the mouse plasma.

As reported previously, debenzylation of **2** and [^{11}C]**2** was a main route of metabolism.[25,28] Since the fluoroethyl analogue [^{18}F]**5** had molecular similarity to and the bioisoteric property of [^{11}C]**2**, it may be metabolized with a similar profile to [^{11}C]**2** (Scheme 1). A radioactive metabolite ([^{18}F]**13**) with a benzyl moiety and nonradioactive metabolite (*N*-(5-fluoro-2-phenoxyphenyl)acetamide (**14**) may be the putative metabolite of [^{18}F]**5**. The debenzylated compound **14** had no affinity for PBR and CBR (IC_{50} > 10 μM).[25] Therefore, the presence of the nonradioactive **14** could not interfere with the specific binding of [^{18}F]**5** to PBR in the brain, even if it passed the BBB and entered the brain. Since no radioactive metabolites including [^{18}F]**13** were detected in the mouse brain homogenates, the chemical structure of [^{18}F]**13** was not further identified. These findings could reveal that although [^{18}F]**5** was extensively metabolized in the plasma, all of the specific binding determined in the monkey brain may be due to this ligand itself and not influenced by its radioactive or nonradioactive metabolite.

Conclusion

To develop PET ligands for imaging PBR in the primate brain, four analogues **4**–**7** for PBR were synthesized and evaluated in this time. The two fluoroalkyl analogues **4** and **5** had higher or same affinities for PBR than the parent compound **2** and had no potency for CBR. The iodomethyl analogue **6** had a moderate affinity for PBR and may become a candidate for a SPECT ligand. The PET ligands [^{18}F]**4** and [^{18}F]**5** were respectively synthesized by the alkylation of the desmethyl precursor **3** with [^{18}F]**8** and [^{18}F]**9** in reproducible radiochemical yields. The distribution patterns of [^{18}F]-**4** and [^{18}F]**5** in mice were consistent with the distribution of PBR. However, compared with [^{18}F]**5**, [^{18}F]**4** exhibited a high accumulation of radioactivity in the bone. The PET image of [^{18}F]**4** in the monkey brain also showed significant radioactivity in the bone, indicating that it was not a useful PET ligand because of its remarkable in vivo defluorination. The uptake of [^{18}F]**5** in the occipital cortex of the monkey brain was 1.5 times higher than that of [^{11}C]**2**, and 6 times (maximum value) higher than that of [^{11}C]**2**. Pretreatment with **1** or **2** significantly reduced the radioactivity levels of [^{18}F]**5** to 20–30% of the control in the brain, suggesting a high specific binding of [^{18}F]**5** to PBR in the monkey brain. No radioactive metabolite of [^{18}F]**5** was detected in the brain although it was metabolized in the plasma by debenzylation. This study has succeeded in developing a potential PET ligand [^{18}F]**5** which has high specific binding for PBR in the monkey brain.

Experimental Section

^{1}H NMR spectra were recorded on a JNM-GX-270 spectrometer (JEOL, Tokyo) with tetramethylsilane as an internal

standard. All chemical shifts (δ) were reported in parts per million (ppm) downfield from the standard. FAB-MS was obtained on a JEOL NMS−SX102 spectrometer (JEOL, Tokyo). Column chromatography was performed using Merck Kieselgel gel 60 F_{254} (70−230 mesh). 18-Fluorine (^{18}F) was produced by the ^{18}O (p, n) ^{18}F nuclear reaction using a CYPRIS HM-18 cyclotron (Sumitomo Heavy Industry, Tokyo). If not otherwise stated, radioactivity was determined with an IGC-3R Curiemeter (Aloka, Tokyo). HPLC was performed using a JASCO HPLC system (JASCO, Tokyo): effluent radioactivity was monitored using a NaI (Tl) scintillation detector system. Samples **2** and **3** were kindly provided by Dr A. Nakazoto (Taisho Pharmaceutical). All chemical reagents with the highest grade commercially available were purchased from Aldrich Chem. (Milwaukee, WI) and Wako Pure Chem. Ind. (Osaka). The animal experiments were carried out according to the recommendations of the committee for the care and use of laboratory animals, National Institute of Radiological Sciences (NIRS).

Chemistry. *N*-(5-Fluoro-2-phenoxyphenyl)-*N*-(2-fluoromethyl-5-methoxybenzyl)acetamide (4). A mixture of **3** (19 mg, 0.05 mmol), FCH_2I (**4**, about 20 mg in 1 mL of CH_3CN), and NaH (4 mg, 0.1 mmol) in DMF (2 mL) was stirred at 0 °C for 5 h. The reaction mixture was quenched with AcOEt and washed with water and a saturated NaCl solution. After the organic layer was dried over Na_2SO_4, the solvent was removed to give a residue. Column chromatography of the residue on silica gel with $CHCl_3$/hexane (1/9) gave **4** (16 mg, 79%) as a white powder; mp: 71−72 °C; ^1H NMR (300 MHz, $CDCl_3$) δ: 7.18−7.40 (2H, m), 6.71−7.13 (8H, m), 6.28−6.44 (1H, m), 5.30 (2H, d, J = 49 Hz), 4.80 (2H, dd, J = 2, 12 Hz), 3.71 (3H, s), 2.12 (3H, s); FABMS (*m/z*): 414.2 (M^+ + 1); Anal. ($C_{23}H_{21}F_2NO_4$) C, H, N.

***N*-(5-Fluoro-2-phenoxyphenyl)-*N*-(2-fluoroethyl-5-methoxybenzyl)acetamide (5).** A mixture of **3** (38 mg, 0.1 mmol), FCH_2CH_2Br (**9**, 25 μL, 0.2 mmol) and NaH (8 mg, 0.2 mmol) in DMF (5 mL) was heated at 80 °C for 8 h. The reaction mixture was quenched with AcOEt, and washed with water and a saturated NaCl solution. After the organic layer was dried over Na_2SO_4, the solvent was removed to give a residue. Column chromatography of the residue on silica gel with $CHCl_3$/hexane (1/13) gave **5** (27 mg, 65%) as a white powder; mp: 54−56 °C; ^1H NMR (300 MHz, $CDCl_3$) δ: 7.26−7.59 (2H, m), 6.22−7.19 (9H, m), 4.88 (2H, dt, J = 4, 41 Hz), 4.65 (2H, dd, J = 2, 12 Hz), 4.12 (2H, dt, J = 4, 27 Hz), 3.80 (3H, s), 2.15 (3H, s); FABMS (*m/z*): 428.2 (M^+ + 1); Anal. ($C_{24}H_{23}F_2NO_4$) C, H, N.

***N*-(5-Fluoro-2-phenoxyphenyl)-*N*-(2-iodomethyl-5-methoxybenzyl)acetamide (6).** A mixture of **3** (19 mg, 0.05 mmol) and CH_2I_2 (**10**, 11 μL, 0.15 mmol) in DMF (5 mL) was stirred at 25 °C for 3 h. The reaction mixture was quenched with AcOEt and washed with water and a saturated NaCl solution. After the organic layer was dried over Na_2SO_4, the solvent was removed to give a residue. Column chromatography of the residue on silica gel with $CHCl_3$/hexane (1/15) gave **6** (8.9 mg, 34%) as a colorless oil; ^1H NMR (300 MHz, $CDCl_3$) δ: 7.18−7.40 (2H, m), 6.15−7.33 (9H, m), 4.81 (dd, J = 2, 12 Hz), 4.70 (2H, s), 3.78 (3H, s), 2.20 (3H, s); FABMS (*m/z*): 524.1 (M^+ + 1); Anal. ($C_{23}H_{21}FINO_4$) C, H, N.

***N*-(5-Fluoro-2-phenoxyphenyl)-*N*-(5-methoxy-2-tosyloxyethylbenzyl)acetamide (7).** A mixture of **3** (19 mg, 0.05 mmol), $TsOCH_2CH_2OTs$ (**11**, 37 mg, 0.1 mmol) and NaH (8 mg, 0.2 mmol) in DMF (5 mL) was stirred at 0 °C for 5 h. The reaction mixture was quenched with AcOEt and washed with water and a saturated NaCl solution. After the organic layer was dried over Na_2SO_4, the solvent was removed to give a residue. Column chromatography of the residue on silica gel with $CHCl_3$/hexane (1/20) gave **7** (14 mg, 46%) as a colorless oil; ^1H NMR (300 MHz, $CDCl_3$) δ: 6.52−7.48 (15H, m), 4.62 (2H, dd, J = 2, 12 Hz), 4.43−4.28 (2H, m), 4.12−3.92 (2H, m), 3.80 (3H, s), 3.36 (3H, s), 2.32 (3H, s); FABMS (*m/z*): 580.3 (M^+ + 1); Anal. ($C_{31}H_{30}FNSO_7$) C, H, N.

Radiosynthesis. [^{18}F]Fluoride ([^{18}F]F$^-$). [^{18}F]F^- was produced by the ^{18}O (p, n) ^{18}F reaction on 10−20 at. % $H_2{}^{18}O$ using 18 MeV protons (14.2 MeV on target) from the cyclotron and separated from [^{18}O]H_2O using Dowex 1-X8 anion-exchange resin in an irradiating room. The [^{18}F]F^- was eluted from the resin with aqueous K_2CO_3 (3.3 mg/0.3 mL) into a vial containing CH_3CN (1.5 mL)/4,7,13,16,21,24-hexaoxa-1,10-diazabicyclo[8,8,8]hexacosane (Kryptofix 222, 25 mg) and transferred into a reaction vessel in a hot cell.

***N*-(5-Fluoro-2-phenoxyphenyl)-*N*-(2-[^{18}F]fluoromethyl-5-methoxybenzyl)acetamide ([^{18}F]4).** [^{18}F]F^- from the irradiating room was transported to a Pyrex glass vessel (5 mL) containing 100 μL of *o*-dichlorobenzene (*o*-DCB), and the [^{18}F]F^- was dried to remove H_2O and CH_3CN at 120 °C for 15 min. After CH_2I_2 (**10**, 100 μL) was added to the radioactive mixture by a helium flow (50 mL/min) at 120 °C, [^{18}F]FCH_2I ([^{18}F]**8**) resulted in this vessel was distilled at once under helium for 3 min and bubbled into another Pyrex glass vessel containing the demethyl precursor (**3**, 1.5 mg) and NaH (10 μL, 1.5 g/20 mL DMF) in anhydrous DMF (300 μL) at −15 °C. After maximum radioactivity was bubbled into the solution, the reaction was terminated by adding CH_3CN/H_2O (6/4, 500 μL). The radioactive mixture was applied to a semipreparative HPLC column. HPLC semipreparative purification was completed on YMC J'sphere ODS−H80 column (10 mm ID × 250 mm) using a mobile phase of CH_3CN/H_2O (60/40) at a flow rate of 6.0 mL/min. The retention time (t_R) for [^{18}F]**4** was 11.2 min, whereas that for **3** was 6.7 min. The radioactive fraction corresponding to [^{18}F]**4** was collected in a sterile flask containing polysorbate (80) (75 μL) and ethanol (150 μL), evaporated to dryness under vacuum, redissolved in 7 mL of sterile normal saline, and passed through a 0.22 μm Millipore filter to obtain the final product. At the end of synthesis (EOS), 180−300 MBq of [^{18}F]**4** was obtained as an iv injectable solution at a beam current of 10−15 μA and 20−25 min proton bombardment.

***N*-(5-Fluoro-2-phenoxyphenyl)-*N*-(2-[^{18}F]fluoroethyl-5-methoxybenzyl)acetamide ([^{18}F]5).** After the [^{18}F]F^- was dried, $BrCH_2CH_2OTf$ (**12**, 8 μL) in *o*-dichlorobenzene (400 μL) was added to the radioactive mixture. The [^{18}F]FCH_2CH_2Br ([^{18}F]**9**) in this vessel was distilled under a helium flow (90−100 mL/min) at 130 °C for 5 min and bubbled into another vessel containing **3** (1.5 mg) and NaH (10 μL, 1.5 g/20 mL DMF) in anhydrous DMF (300 μL) at −15 °C, and the reaction mixture was heated and kept at 120 °C for 10 min. HPLC semipreparative purification was performed on a YMC J'sphere ODS−H80 column (10 mm ID × 250 mm) using a mobile phase of CH_3CN/H_2O (55/45) at a flow rate of 6.0 mL/min. The t_R for [^{18}F]**5** was 14.2 min. At EOS, 570−780 MBq of [^{18}F]**5** was obtained as an iv injectable solution at a beam current of 10−15 μA and 20−25 min proton bombardment.

Radiochemical Purity and Specific Activity Determinations. Radiochemical purity was assayed by analytical HPLC (column: CAPCELL PAK C_{18}, 4.6 mm ID × 250 mm, UV at 254 nm; mobile phase: CH_3CN/H_2O = 6/4). The t_R for [^{18}F]**4** and [^{18}F]**5** was 6.1 and 6.3 min at a flow rate of 2.0 mL/min. The specific activity of [^{18}F]**4** and [^{18}F]**5** was determined by comparison of the assayed radioactivity to the mass associated with the carrier UV peak at 254 nm.

In Vitro Binding Assays. Male Sprague−Dawley rats (n = 4) weighing 220−250 g were killed by decapitation under ether anesthesia, and their brains were quickly removed and frozen on powdered dry ice. Brain sagittal sections (20 μm) were cut on a cryostat microtome (HM560, Carl Zeiss Co., Germany) and thaw-mounted on glass slides (Matsunami Glass Ind., Tokyo), which were then dried at room temperature and stored at −18 °C until use for experiments. The brain sections were preincubated at 25 °C for 20 min in 50 mM Tris-HCl (pH 7.4) buffer. After the preincubation, these sections were incubated at 37 °C for 30 min in the assay buffer containing [^{11}C]**2** (1 nM, specific activity: 110 GBq/μmol) or [^{11}C]flumazenil (1 nM, specific activity: 220 GBq/μmol). To determine the IC_{50} values of **1**, **2**, **4**−**7** for the [^{11}C]**2** (for PBR) or [^{11}C]flumazenil (for CBR) binding, the brain sections were incubated with [^{11}C]**2** or [^{11}C]flumazenil in the presence of increasing concentrations of the corresponding **1**, **2**, **4**−**7** (0.1−1000 nM). Nonradioactive **2** or flumazenil (10 μM) of was used

to determine the nonspecific binding for PBR or CBR. After the incubation, the sections were washed three times for 2 min each time with the cold assay buffer, dipped into cold distilled water, and dried with a stream of warm air (about 50 °C). These sections were then placed in contact with imaging plates (BAS-SR 127, Fuji Photo Film Co. Ltd., Tokyo, Japan) for 60 min to analyze the distribution of their radioactivity with a FUJIX BAS 3000 bioimaging analyzer (Fuji). The region of interest (ROI) on the sections was placed on the cerebellum. PSL data corresponding to the radioactivity on the cerebellum in the presence and absence of the displacement **1**, **2**, **4**–**7** were determined. Specific binding for PBR or CBR was defined as total binding minus binding in the presence of **2** or flumazenil (10 μM). The PSL data corresponding to the specific binding at each compound concentration was calculated as a percentage in relation to the control specific binding, and which were converted to probit values to determine the IC_{50} of each compound. The IC_{50} value was further converted to K_i according to the Cheng–Prusoff equation.[36]

Biodistribution on Mice. A saline solution of ^{18}F-ligand (average of 8 MBq/200 μL) was injected into ddy mice (30–40 g, 9 weeks, male) through the tail vein. Four mice for each time point were sacrificed by cervical dislocation at 5, 15, 30, 60 and 120 min after injection. Whole brain, liver, lung, heart, kidney, adrenal, bone, and blood samples were quickly removed and weighed. The radioactivity present in the various tissues was measured in a Packard autogamma scintillation counter and expressed as a percentage of the injected dose per gram of wet tissue (% ID/g). All radioactivity measurements were corrected for decay.

PET on Monkeys. The PET scan was performed using a high-resolution SHR-7700 PET camera (Hamamatsu Photonics, Hamamatsu, Japan) designed for laboratory animals, which provides 31 transaxial slices 3.6 mm (center-to-center) apart and a 33.1 cm field of view. A male rhesus monkey (*macaca mulatta*) weighing about 5 kg was repeatedly anesthetized with ketanine (Ketalar, 10 mg/kg/h, im) every hour through the session. After transmission scans for attenuation correction were performed for 1 h using a 74 MBq ^{68}Ge-^{68}Ga source. A dynamic emission scan in the 3D acquisition mode was performed for 90 min (2 min × 5 scans, 4 min × 10 scans, 10 min × 4 scans). All emission scan images were reconstructed with a Colsher filter of 4 mm, and circular regions of interest (ROIs) with a 5-mm diameter were placed over the occipital cortex using an image analysis software.[35,36] A solution of [^{18}F]**4** and [^{18}F]**5** (80–85 MBq) was injected iv into the monkey, and time-sequential tomographic scanning was performed on a transverse section of the brain for 180 min. In pretreatment experiments, nonradioactive **2** (1 mg/kg) or **1** (5 mg/kg) was injected at 2 min before the [^{18}F]**5** injection. The time activity curves (TACs) in the occipital cortex were obtained for each scan of the brain.

Metabolite Assay for Mouse Plasma and Brain Tissue. After iv injection of [^{18}F]**4** or [^{18}F]**5** (5–10 MBq/100 μL) into ddy mice (n = 3), these mice were sacrificed by cervical dislocation at 5, 15, 30, or 60 min. Blood (0.7–1.0 mL) and whole brain samples were removed quickly. The blood sample was centrifuged at 15 000 rpm for 1 min at 4 °C to separate plasma (250 μL), which was collected in a test tube containing CH_3CN (500 μL) and a solution of the authentic unlabeled **4** or **5** (1.1 mg/5.0 mL of CH_3CN, 10 μL). After the tube was vortexed for 15 s and centrifuged at 15 000 rpm for 2 min for deproteinization, the supernatant was collected. The extraction efficiency of radioactivity into the CH_3CN supernatant ranged from 70% to 92% of the total radioactivity in the plasma. On the other hand, the cerebellum and forebrain including the olfactory bulb were dissected from the mouse brain and homogenized together in an ice-cooled CH_3CN/H_2O (1/1, 1.0 mL) solution. The homogenate was centrifuged at 15 000 rpm for 1 min at 4 °C, and supernatant was collected. The recovery of radioactivity into the supernatant was 68–87% based on the total radioactivity in the brain homogenate.

An aliquot of the supernatant (100–500 μL) obtained from the plasma or brain homogenate was injected into the HPLC system for radioactivity and analyzed under the same conditions described above except that the mobile phase was CH_3CN/H_2O with a ratio of 1/1. The percent ratio of [^{18}F]ligand (t_R = 10.6 min for [^{18}F]**4** and 11.8 min for [^{18}F]**5**) to total radioactivity (corrected for decay) on the HPLC chromatogram was calculated as % = (peak area for [^{18}F]ligand/total radioactive peak area) × 100.

Metabolite Analysis for Monkey Plasma. After iv injection of [^{18}F]**5** (80 MBq) into the monkey, arterial blood samples (1 mL) were collected at 2, 10, 30, 60, 90, 120, and 180 min. All samples were centrifuged at 15 000 rpm for 1 min at 4 °C to separate plasma (250 μL), which was collected in a test tube containing CH_3CN (0.5 mL). The tube was vortexed for 15 s and centrifuged at 15 000 rpm for 1 min for deproteinization. The extraction efficiency of radioactivity into the CH_3CN ranged from 73% to 94% of the total radioactivity in the plasma. The radioactive fractions in these samples were determined using HPLC.

Acknowledgment. The authors are grateful to Dr A. Nakazoto (Taisho Pharmaceutical Co., Ltd.) for providing the samples (**2** and **3**) and helpful suggestions. We also thank the crew of the Cyclotron Operation Section and Radiopharmaceutical Chemistry Section of National Institute of Radiological Sciences (NIRS) for support in operation of the cyclotron and production of radioisotopes.

Supporting Information Available: Radioactivity distribution of [^{18}F]**4** and [^{18}F]**5**. This material is available free of charge via the Internet at http://pubs.acs.org.

References

(1) Braestrop, C.; R. F. Squires Specific Benzodiazepine Receptors in Rat Brain Characterized by High Affinity [^{3}H]Diazepam Binding. *Proc. Natl. Acad. Sci. U.S.A.* **1977**, *74*, 1839–1847.
(2) Anholt, R. R. H.; DeSouza, E. B.; Oster-Granite, M. L.; Synder, S. H. Peripheral-type Benzodiazepine Receptors: Autoradiographic Localization in Whole-body Sections of Neonatal Rats. *J. Pharmacol. Exp. Ther.* **1985**, *233*, 517–526.
(3) Gavisg, M.; Katz, Y.; Bar-Ami, S.; Wizman, R. Biochemical, Physiological and Pathological Aspects of the Peripheral Benzodiazepine Receptor. *J. Neurochem.* **1992**, *58*, 1589–1602.
(4) Schoemaker, H.; Bliss, M.; Yamamura, H. I. Specific High Affinity Saturable Binding to [^{3}H]Ro5–4864 Benzodiazepine Binding Sites in Rat Cerebral Cortex. *Eur. J. Pharmacol.* **1981**, *71*, 473–475.
(5) Weissman, B. A.; Gordon, T. B.; Lawrence, I.; Steven, M. P.; Stolnick, P. Characterization of the Binding of [^{3}H]Ro 5–4864, a Convulsant Benzodiazepine, to Guinea Pig Brain. *J. Neurochem.* **1984**, *42*, 969–975.
(6) Zisterer, D. M.; Williams, D. C. Peripheral-type Benzodiazepine Receptors. *Gen. Pharmacol.* **1997**, *29*, 305–314.
(7) Benavides, J.; Fage, D.; Carter, C.; Scatton, B. Peripheral Type Benzodiazepine Binding Sites are a Sensitive Indirect Index of Neuronal Damage. *Brain Res.* **1987**, *421*, 167–172.
(8) Diorio, D.; Welner, S.; Butterworth, R.; Meaney, M.; Suranyl-Cadotte, R. Peripheral Benzodiazepine Binding Sites in Alzheimer's Disease Frontal Cortex and Temporal Cortex. *Neurobiol. Aging* **1991**, *12*, 255–258.
(9) Messmer, K.; Reynolds, G. P. Increased Peripheral Benzodiazepine Binding Sites in the Brain of Patients with Huntington's Disease. *Neurosci. Lett.* **1998**, *241*, 53–56.
(10) Deajardins, P.; Todd, K. G.; Hazell, H. A.; Butterworth, R. F. Increased "Peripheral-type" Benzodiazepine Receptor Sites and mRNA in Thalamus of Thiamine Deficient Rats. *Neurochem. Int.* **1999**, *35*, 363–369.
(11) Banati R. B.; Newcombe, J.; Gunn, R. N.; Cagnin, A.; Turkheimer, F.; Heppner, F.; Price, G.; Wegner, F.; Giovannoni, G.; Miller, D. H.; Perkin, G. D.; Smith, T.; Hewson, A. K.; Bydder, G.; Kreutzberg, G. W.; Jones, T.; Cuzner, M. L.; Myers, R. The Peripheral Benzodiazepine Binding Site in the Brain in Multiple Sclerosis: Quantitative In Vivo Imaging of Microglia as a Measure of Disease Activity. *Brain* **2000**, *123*, 2321–2337.
(12) Raghavendra Rao, V. L.; Dogan, A.; Bowen, K. K. Dempsy, R. J. Traumatic Brain Injury Leads to Increased Expression of peripheral-type Benzodiazepine Receptors, neuronal Death, and Activation of Astrocytes and Microglia in Rat Thalamus. *Exp. Neurol.* **2000**, *161*, 102–114.

(13) Johnson, E. W.; De Ianerolle, N. C.; Kim, J. H.; Sundaresan, S.; Spencer, D. D.; Mattson, R. H.; Zoghbi, S. S.; Baldwin, R. M.; Hoffer, P. B.; Seibyl, J. P. "Central" and "Peripheral" Benzodiazepine Receptors: Opposite Changes in Human Epileptogenic Tissue. *Neurology* **1992**, *42*, 811−815.
(14) Sauvageau, A.; Desjardins, P.; Lozeva, V.; Rose, C.; Hazell, A. S.; Bouthillier, A.; Butterwort, R. F. Increased Expression of "Peripheral-type" Benzodiazepine Receptors in Human Temporal Lobe Epilepsy: Implications for PET Imaging of Hippocampal Sclerosis. *Metab. Brain. Dis.* **2002**, *17*, 3−11.
(15) Camsonne, R.; Crouzel, C.; Comar, D.; Maziere, M.; Prenant, C.; Sastre, J.; Moulin, M. A.; Syrota, A. Synthesis of N-[^{11}C]-Methyl, N−(Methyl-1-propyl), (Chloro-2-phenyl)-1-isoquinoline Carboxamide-3 (PK11195): a New Ligand for Peripheral Benzodiazepine Receptors. *J. Labelled Comp. Radiopharm.* **1984**, *21*, 985−991.
(16) Hashimoto, K.; Inoue, O.; Suzuki, K.; Yamasaki, T.; Kojima, M., 1989. Synthesis and Evaluation of ^{11}C−PK 11195 for In Vivo Study of Peripheral-type Benzodiazepine Receptors Using Positron Emission Tomography. *Ann. Nucl. Med.* **1989**, *3*, 63−71.
(17) Cappelli, A.; Anzini, M.; Vomero, S.; De Benedetti, P. G.; Menziani, M. C.; Giorgi, G.; Manzoni, C. Mapping the Peripheral Benzodizaepine Receptor Binding Site by Conformationally Restrained Derivatives of 1-(2-Chlorophenyl)-1-*N*-methypropyl-3-isoquinolinecarboxamide (PK11195). *J. Med. Chem.* **1997**, *40*, 2910−2921.
(18) Matarrese, M.; Moresco, R. M.; Cappelli, A.; Anzini, M.; Vomero, S.; Simonelli, P.; Verza, E.; Magni, F.; Sudati, F.; Soloviev, D.; Todde, S.; Carpinelli, A.; Kienle, M. G.; Fazio, F. Labeling and Evaluation of N-[^{11}C]Methylated Quinoline-2-carboxamides as Potential Radioligands for Visualization of Peripheral Benzodiazepine Receptors. *J. Med. Chem.* **2001**, *44*, 579−585.
(19) Pike, V. W.; Halldin, C.; Crouzel, C.; Barre, L.; Nutt, D. J.; Osman, S.; Shah, F.; Turton, D. R.; Waters, S. L. Radioligands for PET Studies of Central Benzodiazepine Receptors and PK (Peripheral Benzodiazepine) Binding Sites-Current Status. *Nucl. Med. Biol.* **1993**, *20*, 503−525.
(20) Pappata, P.; Cornu, Y.; Samson, C.; Prenant, J.; Benavides, B.; Scatton, C.; Crouzel, J. J.; Hauw, A.; Syrota, A. PET Study of Carbon-11-PK11195 Binding to Peripheral Type Benzodiazepine Sites in Glioblastoma: a Case report. *J. Nucl. Med.* **1991**, *32*, 1608−1610.
(21) Cagnin, A.; Brooks, D. J.; Kennedy, A. M., Gunn, R. N.; Myers, R.; Turkheimer, F. E.; Jones, T.; Banati, R. B. In-vivo Measurement of Activated Microglia in Dementia. *Lancet* **2001**, *358*, 461−467.
(22) Banati, R. B.; Goerres, G. W.; Myers, R.; Gunn, R. N.; Turkheimer, F. E.; Kreutzberg, G. W.; Brooks, D. J., Jones, T.; Duncan, J. S. [^{11}C](R)-PK11195 Positron Emission Tomography Imaging of Activated Microglia In Vivo in Rasmussen's encephalitis. *Neurology* **1999**, *53*, 2199−2203.
(23) Debruyne, J. C.; Van Laere, K. J.; Versijpt, J.; De Vos, F.; Eng, J. K.; Strijckmans, K.; Santens, P.; Achten, E.; Slegers, G.; Korf, J.; Dierckx, R. A.; De Reuck, J. L. Semiquantification of the Peripheral-type Benzodiazepine Ligand [^{11}C]PK11195 in Normal Human Brain and Application in Multiple Sclerosis Patients. *Acta Neurol. Belg.* **2002**, *102*, 127−135.
(24) Nakazato, A.; Okubo, T.; Nakamura, T.; Chaki, S.; Tomisawa, K.; Nagamine, M.; Yamamoto, K.; Harada, K.; Yoshida, M. Aryloxyaniline derivatives. WO99/06353.
(25) Chaki, S.; Funakoshi, T.; Yoshikawa, R.; Okuyama, S.; Okubo, T.; Nakazato, A.; Naganine, M.; Tomisawa, K. Binding Characteristics of [^{3}H]DAA1106, a Novel and Selective Ligand for Peripheral Benzodiazepine Receptors. *Eur. J. Pharmacol.* **1999**, *371*, 197−204.
(26) Okuyama, S.; Chaki, S.; Yoshikawa, R.; Ogawa, S.; Suzuki, Y.; Okubo, T.; Nakazato, A.; Nagamine, M.; Tomisawa, K. Neuropharmacological Profile of Peripheral Benzodiazepine Receptor Agonists, DAA1097 and DAA1106. *Life Sci.* **1999**, *64*, 1455−1564.
(27) Okubo, T.; Yoshikawa, R.; Chaki, S.; Okuyama, S.; Nakazato, A. Design, synthesis and structure-affinity relationships of aryloxyanilide derivatives as novel peripheral benzodiazepine receptor ligands. *Bioorg. Med. Chem.* **2004**, *12*, 423−438.
(28) Zhang, M.-R.; Kida, T.; Noguchi, J.; Furutsuka, K.; Maeda, J.; Suhara, T.; Suzuki, K.; [^{11}C]DAA1106: Radiosynthesis and In Vivo Binding to Peripheral Benzodiazepine Receptors in Mouse Brain. *Nucl. Med. Biol.* **2003**, *30*, 513−519.
(29) Maeda, J.; Suhara, T.; Zhang, M.-R.;Okauchi, T.; Yasuno, F.; Ikoma, Y.; Inaji, M.; Nagai, Y.; Ichimiya,; Ohbayashi, S.; Suzuki, K. Novel Peripheral Benzodiazepine Receptor Ligand [^{11}C]-DAA1106 for PET; An Imaging Tool for Glial Cells in the Brain. *Synapse*, in press.
(30) Zhang, M.-R.; Maeda, J.; Furutsuka, K.; Yoshida, Y.; Ogawa, M.; Suhara, T.; Suzuki, K. [^{18}F]FMDAA1106 and [^{18}F]-FEDAA1106: Two Positron-emitter Labeled Ligands for Peripheral Benzodiazepine Receptor (PBR). *Bioorg. Med. Chem. Lett.* **2003**, *13*, 201−204.
(31) Zheng, L.; Berridge, M. S. Synthesis of [^{18}F]fluoromethyl Iodide, a Synthetic precursor for Fluoromethylation of Radiopharmaceutical. *Appl. Radiat. Isot.* **2000**, *52*, 55−61.
(32) Zhang, M.-R.; Tsuchiyama, A.; Haradahira, T.; Yoshida, Y.; Furutsuka, K.;Suzuki, K. Development of an Automated System for Synthesizing ^{18}F-Labeled Compounds Using [^{18}F]Fluoroethyl Bromide as a Synthetic Precursor. *Appl. Radiat. Isot.* **2002**, *57*, 335−342.
(33) Zhang, M.-R.; Ogawa, M.; Furutsuka, K.; Yoshida, Y.; Suzuki, K. [^{18}F]Fluoromethyl Iodide ([^{18}F]FCH_2I): Preparation and Reactions with Phenol, Thiophenol, Amide and Amine Functional Groups. *J. Fluorin. Chem.*, accepted.
(34) Silver, S.; Sihver, W.; Bergstrom, M.; Hoglund, U.; Sjoberg, P.; Langstrom, B.; Watanabe, Y. Quantitative Autoradiography with Short-lived Positron Emission Tomography Tracers: a Study on Muscarinic Acetylcholine Receptors with *N*-[^{11}C]Methyl-4-piperidylbenzilate. *J. Pharmacol. Exp. Ther.* **1999**, *290*, 917−922.
(35) Zhang, M.-R.; Haradahira, T.; Maeda, J.; Okauchi, T.; Kawabe, K.; Kida, T.; Obayashi, S.; Suzuki K.; Suhara T. Synthesis and Evaluation of 3-(4-Chlorobenzyl)-8-[^{11}C]methoxy-1,2,3,4-tetrahydrochromeno[3,4-c]pyridin-5-one: a PET Tracer for Imaging Sigma$_1$ Receptors. *Nucl. Med. Biol.* **2002**, *29*, 469−476.
(36) Petit-Taboué, M. C.; Baron, J. C.; Barré, L.; Travère, J. M.; Speckel, D.; Camsonne, R.; MacKenzie, E. T. Brain Kinetics and Specific Binding of [^{11}C]PK 11195 to Omaga3 Sites in Baboons: Positron Emission Tomography Study. *Eur. J. Pharmacol.* **1991**, *200*, 347−351.
(37) Cheng, Y. C.; Prusoff, W. H. Relationship between Inhibition Constant (Ki) and the Concentration of Inhibitor Which Causes 50 Percent Inhibition (IC50) of an Enzymatic Reaction. *Biochem. Pharmacol.* **1973**, *92*, 881−894.
(38) Maeda, J.; Suhara, T.; Kawabe, K.; Okauchi, T.; Obashi S.; Hojo J.; Suzuki K. Visualization of α5 Subunit of $GABA_A$/Benzodiazepine Receptor by [^{11}C]Ro15−4513 Using Positron Emission Tomography. *Synapse.* **2003**, *47*, 200−208.

JM0304919

Synthesis of ^{11}C-Labelled Bis(phenylalkyl)amines and Their *in Vitro* and *in Vivo* Binding Properties in Rodent and Monkey Brains

Shigeki SASAKI,[a,c] Fumie KUROSAKI,[a] Terushi HARADAHIRA,[b,c] Fumihiko YAMAMOTO,[a,c] Jun MAEDA,[b] Takashi OKAUCHI,[b] Kazutoshi SUZUKI,[b] Tetsuya SUHARA,[b,c] and Minoru MAEDA*[,a,c]

[a] *Graduate School of Pharmaceutical Sciences, Kyushu University; 3-1-1 Maidashi, Higashi-ku, Fukuoka 812-8582, Japan:* [b] *National Institute of Radiological Sciences; 4-9-1 Anagawa, Inage-ku, Chiba 263-8555, Japan: and* [c] *CREST, Japan Science and Technology Corporation; 4-1-8 Honmachi, Kawaguchi, Saitama 332-0012, Japan.*
Received December 15, 2003; accepted January 24, 2004

Two new ^{11}C-labelled ligands, *N*-(3-(4-hydroxyphenyl)propyl)-3-(4-methoxyphenyl)propylamine ([^{11}C]2) and *N*-(3-(4-hydroxyphenyl)butyl)-3-(4-methoxyphenyl)butylamine ([^{11}C]3) were designed based on bis(phenylalkyl)-amines (1) which have been reported as polyamine site antagonists with high-selectivity for NR1A/2B NMDA receptors, and radiolabelling of the corresponding phenol precursors with [^{11}C]methyl iodide was readily accomplished. The *in vitro* inhibition experiments using rat brain slices showed that [^{11}C]2 and [^{11}C]3 share the binding sites with spermine and/or ifenprodil but not with CP-101,606, a highly potent NR2B-selective NMDA antagonist, and that divalent cations such as Zn^{2+} produced significant inhibition of both [^{11}C]2 and [^{11}C]3 bindings. Intravenous injection of [^{11}C]3 in mice showed almost homogenous distribution throughout the brain. Attempts to block the tracer uptake of [^{11}C]3 by pre-injection with the unlabelled 3 or spermine in rats were unsuccessful, but a small decrease in the cerebral uptake of [^{11}C]3 by co-treatment with the unlabelled 3 was observed in a monkey PET study. The present findings indicate that none of these ^{11}C-labelled analogues have potential for PET study of binding sites on the *N*-methly-D-aspartate (NMDA) receptors.

Key words *N*-methly-D-aspartate (NMDA) receptor antagonist; ^{11}C-labelling; brain distribution; inhibition experiment; bis(phenylalkyl)amine; polyamine binding site

The *N*-methyl-D-aspartate (NMDA) class ionotropic receptors for glutamate play a central role in excitatory neurotransmission in the central nervous system (CNS). Some CNS disorders such as ischemic, hypoxic, hypoglycemic, and traumatic insults, epilepsy, AIDS, dementia, and Huntington's and Alzheimer's diseases are accompanied by disorders of the NMDA receptors.[1—8] For non-invasive diagnoses of NMDA receptor dysfunctions by PET (positron emission tomography), a number of radioactive ligands labelled with short-lived ^{18}F ($t_{1/2}$=109.7 min) or ^{11}C ($t_{1/2}$=20.3 min) have been investigated. However, efforts have been limited by poor brain entry or high levels of nonspecifc binding.[9] Native NMDA receptors are present as complexes containing at least one NR1 subunit and one or more of the four distinct NR2 subunits (NR2A-D), with a number of recognition sites for endo- and exogeneous ligands that modulate neuronal responses.[10,11] Recently, a series of bis(phenylalkyl)amines (**1**), structural analogues of ifenprodil, were reported as polyamine site antagonists with high-selectivity for NR2B containing NMDA receptors, as exemplified by compound (**1**) (Fig. 1, m=5, n=2, IC_{50}=8 nM for the NR1A/2B subunit combination).[12—15] There are at least three independent polyamine-binding sites on the NMDA receptors—the glycine-dependent modulatory site, the glycine-independent modulatory site, and the voltage-dependent ion channel site.[16—22] The bis(phenylalkyl)amines have been shown to bind to the glycine-independent polyamine modulatory site, which is absolutely required for the NR2B subunit.[23] It has been reported that the primary determinants of potency of the bis(phenylalkyl)amines (**1**) at the NR1A/2B NMDA receptors are (1) the phenolic OH group; (2) the distance between the two aromatic rings; and (3) the nitrogen atom.[15] Thus, we designed mono [^{11}C]methoxyl derivatives of **1**. In this study, we synthesized two ^{11}C-labelled analogues of bis(phenylalkyl)amine, bis(phenylpropyl)amine ([^{11}C]**2**) and bis(phenylbutyl)amine ([^{11}C]**3**), and examined their *in vitro* and *in vivo* binding properties in rodent and monkey brains.

MATERIALS AND METHODS

Radioactivity was quantified with a IGC-3R Curiemeter (Aloka). High-pressure liquid chromatography (HPLC) was done using a JASCO HPLC system for radioactive runs. Effluent radioactivity from the HPLC was determined using a NaI(Tl) scintillation detector system. Carbon-11 was generated by the ^{14}N(p,α)^{11}C nuclear reaction using a CYPRIS-HM-18 Cyclotron (Sumitomo Heavy Industries, Ltd). All animal studies were carried out in compliance with the Animal Ethical Committee of the National Institute of Radiological Sciences and Japanese law. The preparation of [^{11}C]CH_3I and subsequent ^{11}C-methylations were carried out automatically by using a synthetic apparatus for ^{11}C-labelled compounds developed by Suzuki *et al.*[24] ^{1}H-NMR spectra were obtained on a JNM GX-270 spectrometer with TMS as an internal standard, and IR spectra were recorded with a JASCO IR Report 100 spectrometer. Low-resolution FAB mass spectra

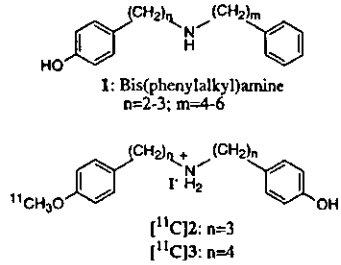

Fig. 1. Structure of Bis(phenylalkyl)amines **1**—**3**

* To whom correspondence should be addressed. e-mail: maeda@phar.kyushu-u.ac.jp

were obtained on a JEOL JMS-D300 spectrometer, and high-resolution FAB (HR-FAB-MS) mass spectra were obtained on a JEOL NMS-SX 102-SX spectrometer. Column chromatography was done on a Merck Kieselgel 60 (70—230 mesh) or Fuji gel FL-60D. Thin-layer chromatography (TLC) was carried out on Merck Kieselgel 60 F_{254} plates. Melting points were determined on a Yanagimoto melting point apparatus and are uncorrected. Elemental analyses were performed by the staff of the micro-analysis section of Kyushu University.

All chemicals were used without further purification unless otherwise stated. Three polyamine (spermine, spermidine, putrescine) hydrochlorides, L-glutamic acid hydrochloride, glycine, ifenprodil tartrate, 5,7-dichlorokynurenic acid (DCKA), CGS-19755, 8-OH-DPAT hydrobromide, prazosin hydrochloride and ketanserin tartrate, were purchased from Sigma Chemical Co. 1,3-Di-*o*-tolylguanidine (DTG) was purchased from Aldrich Chemical Co.

Synthesis of 1-*p*-Toluenesulfonyloxy-3-(4-methoxyphenyl)-propane (4) *p*-Toluenesulfonyl chloride (6.3 g, 33 mmol) was added to a solution of 3-(4-methoxyphenyl)propanol (5 g, 30 mmol) in anhydrous pyridine (75 ml) at 0 °C. The reaction mixture was stirred at 4 °C for 16 h, then added to a solution of conc. HCl and ice (1/1, 100 ml). The resulting solution was extracted with Et_2O (300 ml). The separated organic layers were washed with brine, dried over anhydrous Na_2SO_4, filtered, and concentrated *in vacuo*. The residue was purified by chromatography on a silica gel column (hexane : AcOEt = 5 : 1) to give **4** as a white solid (9.0 g, 94%): mp 38—39 °C; ^{1}H-NMR ($CDCl_3$) δ: 1.88—1.96 (2H, m), 2.44 (3H, s), 2.58 (2H, t, J=7.4 Hz), 3.76 (3H, s), 4.01 (2H, t, J=6.1 Hz), 6.77 (2H, d, J=8.9 Hz), 6.97 (2H, d, J=8.6 Hz), 7.33 (2H, d, J=7.9 Hz), 7.78 (2H, d, J=8.6 Hz); IR (neat) cm^{-1}: 1355; *Anal.* Calcd for $C_{17}H_{20}O_4S$: C, 63.73; H, 6.29. Found. C, 63.86; H, 6.34.

Synthesis of 1-*p*-Toluenesulfonyloxy-3-(4-methoxyphenyl)-butane (5) *p*-Toluenesulfonyl chloride (6.1 g, 32 mmol) was added to a solution of 4-(4-methoxyphenyl)butanol (4.7 ml, 27 mmol) in anhydrous pyridine (75 ml) at 0 °C. The reaction mixture was stirred at 4 °C for 18 h. The work-up and purification were carried out as described above to produce **5** as a colorless oil (7.3 g, 81%): ^{1}H-NMR ($CDCl_3$) δ: 1.59—1.68 (4H, m), 2.44 (3H, s), 2.50 (2H, t, J=7.1 Hz), 3.78 (3H, s), 4.03 (2H, t, J=6.1 Hz), 6.80 (2H, d, J=8.9 Hz), 7.01 (2H, d, J=8.6 Hz), 7.33 (2H, d, J=7.9 Hz), 7.78 (2H, d, J=8.3 Hz); IR (neat) cm^{-1}: 1350; FAB Mass (*m/z*): 334 $(M)^+$.

Synthesis of *N*,*N*-Bis(3-(4-methoxyphenyl)propyl)-*p*-toluenesulfonamide (6) A solution of *p*-toluenesulfonamide (1 g, 6.1 mmol) and 60% sodium hydride oil suspension (488 mg, 12.2 mmol) in anhydrous DMF (35 ml) was heated at 40—45 °C for 1 h, followed by the addition of **4** (3.5 g, 10.9 mmol) in three portions over 2 h at 50—55 °C, and the reaction mixture was stirred at 50—55 °C for 1 h. The reaction mixture was diluted with water (35 ml), and extracted with toluene. The separated organic layers were washed with brine, dried over anhydrous Na_2SO_4, filtered, and concentrated *in vacuo*. The residue was purified by chromatography on a silica gel column (hexane : AcOEt = 5 : 1) to give **6** as a white solid (1.68 g, 66%): mp 67—68 °C; ^{1}H-NMR ($CDCl_3$) δ: 1.78 (4H, quintet, J=7.7 Hz), 2.41 (3H, s), 2.49 (4H, t, J=7.6 Hz), 3.10 (4H, t, J=7.8 Hz), 3.79 (6H, s), 6.81 (4H, d, J=8.9 Hz), 7.03 (4H, d, J=8.9 Hz), 7.26 (2H, d, J=7.9 Hz), 7.62 (2H, d, J=8.3 Hz); *Anal.* Calcd for $C_{27}H_{33}NO_4S$: C, 69.35; H, 7.11; N, 3.00. Found. C, 69.32; H, 7.14; N, 3.01.

Synthesis of *N*,*N*-Bis(3-(4-methoxyphenyl)butyl)-*p*-toluenesulfonamide (7) A solution of *p*-toluenesulfonamide (1 g, 5.88 mmol) and 60% sodium hydride oil suspension (484 mg, 12.1 mmol) in anhydrous DMF (35 ml) was heated at 40—45 °C for 1 h, followed by the addition of **5** (3.5 g, 10.5 mmol) in three portions over 2 h at 50—55 °C. After the reaction at 50—55 °C for 1 h, the reaction mixture was worked up and purified as described above to give **7** as a colorless oil (1.91 g, 74%): ^{1}H-NMR ($CDCl_3$) δ: 1.47—1.53 (8H, m), 2.40 (3H, s), 2.51 (4H, t, J=6.9 Hz), 3.07 (4H, t, J=6.9 Hz), 3.78 (6H, s), 6.81 (4H, d, J=8.6 Hz), 7.05 (4H, d, J=8.6 Hz), 7.25 (2H, d, J=7.6 Hz), 7.64 (2H, d, J=8.3 Hz); FAB Mass (*m/z*): 496 $(M+H)^+$.

Synthesis of *N*,*N*-Bis(3-(4-hydroxyphenyl)propyl)amine Hydrobromide (8) A solution of **6** (500 mg, 1.07 mmol) in AcOEt (10 ml) was added to a solution of phenol (10 g, 107 mmol) in 30% HBr/AcOH (194 ml). The reaction mixture was stirred at room temperature for 18 h, then cooled in an ice bath, followed by the addition of water (200 ml). The aqueous layer was washed with Et_2O, and concentrated *in vacuo*. The residue was purified by chromatography on a silica gel column (chloroform : methanol = 9 : 1) to give **8** as a brown powder (244.8 mg, 63%): mp 165—168 °C; ^{1}H-NMR (CD_3OD) δ: 1.91 (4H, quintet, J=7.7 Hz), 2.59 (4H, t, J=7.4 Hz), 2.94 (4H, t, J=7.9 Hz), 6.70 (4H, d, J=8.6 Hz), 7.01 (4H, d, J=8.2 Hz); IR (neat) cm^{-1}: 3425; HR-FAB-MS (*m/z*); Calcd for $C_{18}H_{24}NO_2$ (M+H): 286.1807. Found. 286.1828.

Synthesis of *N*,*N*-Bis(3-(4-hydroxyphenyl)butyl)amine Hydrobromide (9) A solution of **7** (500 mg, 1.00 mmol) in AcOEt (10 ml) was added to a solution of phenol (10 g, 107 mmol) in 30% HBr/AcOH (194 ml). The reaction mixture was stirred at room temperature for 18 h, worked up and the crude product was purified as described above to give **9** as a brown powder (156.6 mg, 40%): mp 213—217 °C; ^{1}H-NMR (CD_3OD) δ: 1.62—1.65 (8H, m), 2.56 (4H, t, J=6.9 Hz), 2.92 (4H, t, J=7.6 Hz), 6.69 (4H, d, J=8.6 Hz), 7.00 (4H, d, J=8.6 Hz); IR (neat) cm^{-1}: 2400—3500; HR-FAB-MS (*m/z*); Calcd for $C_{20}H_{28}NO_2$ (M+H): 314.2120. Found. 314.2101.

Synthesis of *N*-(3-(4-Hydroxyphenyl)propyl)-3-(4-methoxyphenyl)propylamine (2) The hydrobromide (**8**) was added to a saturated aqueous solution of $NaHCO_3$, and the corresponding free amine was extracted with ether. The organic layers were washed with brine, dried over anhydrous Na_2SO_4, filtered, and concentrated *in vacuo*. Sodium hydride (60% suspension in oil, 2.7 mg, 0.068 mmol) was added to a solution of the above free amine (white powder, 9.5 mg, 0.033 mmol) in anhydrous DMF (1 ml), and the mixture was stirred for 5 min, followed by the addition of methyl iodide (2.1 μl, 0.033 mmol). After the reaction mixture was stirred for 20 min, it was quenched by the addition of 10% aqueous acetic acid, and neutralized with saturated aqueous $NaHCO_3$, then extracted with Et_2O. The separated organic layers were washed with brine, dried over anhydrous Na_2SO_4, filtered, and concentrated *in vacuo*. The residue was purified by HPLC (column: nacalai tesque COSMOSIL 5C18-MS,

10×250 mm, 0.05% trifluoroacetic acid in methanol: H_2O=3 : 2, UV monitor 254 nm, flow rate 4.0 ml/min) to give **2** as a yellow oil (7.3 mg, 74%). ^{1}H-NMR (CD_3OD) δ: 1.87—1.93 (4H, m), 2.61 (4H, dd, J=7.8 Hz), 2.92 (4H, t, J=8.1 Hz), 3.75 (3H, s), 6.71 (2H, d, J=8.9 Hz), 6.84 (2H, d, J=8.9 Hz), 7.01 (2H, d, J=8.6 Hz), 7.11 (2H, d, J=8.9 Hz); HR-FAB-MS (*m/z*); Calcd for $C_{19}H_{26}NO_2$ (M+H): 300.1964. Found. 300.1954.

Synthesis of *N*-(3-(4-hydroxyphenyl)butyl)-3-(4-methoxyphenyl)butylamine (3) The free amine form was obtained from **9** as described above. Monomethylation of the resulting white powder (7.6 mg, 0.024 mmol) and purification were carried out as described above to give **3** as a yellow oil (2.5 mg, 32%). ^{1}H-NMR (CD_3OD) δ: 1.57—1.65 (8H, m), 2.61 (4H, t, J=6.8 Hz), 2.90—2.95 (4H, m), 3.73 (3H, s), 6.69 (2H, d, J=8.6 Hz), 6.82 (2H, d, J=8.6 Hz), 6.99 (2H, d, J=8.6 Hz), 7.09 (2H, d, J=8.6 Hz); HR-FAB-MS (*m/z*); Calcd for $C_{21}H_{30}NO_2$ (M+H): 328.2277. Found. 328.2290.

Radiosynthesis of *N*-(3-(4-Hydroxyphenyl)propyl)-3-(4-[^{11}C]methoxyphenyl)propylamine ([^{11}C]2) and *N*-(3-(4-Hydroxyphenyl)butyl)-3-(4-[^{11}C]methoxyphenyl)butylamine ([^{11}C]3) The free base (0.9 mg) of **8** or **9** in anhydrous DMF (300 μl) was reacted with [^{11}C]CH_3I in the presence of four equivalents of NaH in anhydrous DMF (1 μl) at 30 °C for 3 min. After the HPLC mobile phase (500 μl) (MeOH : 0.05%CF_3COOH=45 : 55 for [^{11}C]**2**, or MeOH : 0.05%CF_3COOH=48 : 52 for [^{11}C]**3**) had been added, the reaction mixture was transferred onto a reverse phase HPLC (column: Waters μ-Bondapak C18, 7.8×300 mm) and eluted with the corresponding mobile phases at a flow rate of 3 ml/min. The radioactive peaks corresponding to the desired products (t_R=*ca.* 10 min for [^{11}C]**2**, or t_R=*ca.* 9.5 min for [^{11}C]**3**) were collected in a flask, respectively. After the solvents were removed under reduced pressure, distilled water or isotonic saline was added to the flask and used for *in vitro* or *in vivo* experiments. An aliquot was assayed for radioactivity and checked by HPLC (column: Waters μ-Bondapak C18, 3.9×300 mm). The mobile phases were MeOH : 0.05%CF_3COOH=45 : 55 at 0.7 ml/min for [^{11}C]**2** and MeOH : 0.05%CF_3COOH=50 : 50 at 0.8 ml/min for [^{11}C]**3**, respectively. The identity of the products was achieved by HPLC co-injection with authentic **2** or **3**. Specific radioactivity at the end of synthesis was calculated by UV spectroscopy. The averages 1.2 GBq of [^{11}C]**2** and 1.6 GBq of [^{11}C]**3** were obtained in a total synthesis of 20—25 min from the end of bombardment after a 10 min proton bombardment at a beam current of 15 μA, respectively.

***In Vitro* Binding on Rat Brain Slices** Autoradiography on rat brain slices was performed essentially as has been previously described.[25] Brain sagittal cryosections (20 μm) obtained from male Sprague–Dawley rats (10—12 weeks old) were pre-incubated in a 50 mM Tris–HCl buffer (pH=7.4) at 25 °C for 30 min, followed by incubation in the same buffer containing [^{11}C]**2** or [^{11}C]**3** (*ca.* 18 MBq, 1—2 nM) for 40 min at 25 °C. The sections were washed three times for 2 min each with a cold incubation buffer, dipped into cold water, dried under a stream of warm air, and placed in contact with ^{11}C-sensitive imaging plates (BAS-SR 127, Fujiphoto Film) for 60 min to analyze their radioactivity of distribution on the slices with a BAS 3000 imaging analyzer (Fujiphoto Film). Radioactivity in regions of interest (ROI) on the slices was recorded as photostimulated luminescence (PSL) values per mm^2 which are proportional to the radioactivity of the measured sample,[26] and was expressed as region-to-cerebellum ratios calculated by dividing the PSL values in each brain region by the cerebellum PSL value on the same slice. Background PSL values were always subtracted from the total PSL values on ROI. Nonradioactive **2** or **3** (100 μM) were simultaneously incubated with the corresponding radioligand to determine their nonspecific binding.

Drug Inhibition for *in Vitro* Binding The rat brain sagittal sections were incubated at 25 °C for 40 min in a 50 mM Tris–HCl buffer containing [^{11}C]**2** or [^{11}C]**3** (*ca.* 18 MBq, 1—2 nM) without or with drugs (10, 100 μM, or 1 mM). Following the incubation, the sections were rinsed, dried and apposed to the imaging plates for 60 min in the same manner as described above. A region of interest (ROI) on the slices was placed on the frontal cortex and the radioactivity in this region was expressed as photostimulated luminescence (PSL) values per mm^2. The PSL data on the ROI in the presence of drugs were divided by the corresponding control PSL data in the absence of drugs. Background PSL values were subtracted from the total PSL values on ROI. The obtained % control values (defined as 100% for the ^{11}C-ligand binding activity in the absence of drugs) were averaged in at least triplicate sections from three animals.

***In Vivo* Brain Distribution** [^{11}C]**3** (in 0.2 ml water, *ca.* 55 MBq/ml) was injected *via* a tail vein into ddY mice (36—38 g). The animals were killed at 10, 30 and 50 min by decapitation. Their whole brains were rapidly removed and dissected into the cerebellum, cerebral cortex, hippocampus, and striatum. A sample of blood was also taken. Radioactivity in each sample was measured with a Packard gamma-counter and corrected for decay. The results were expressed as the percentage of injected dose per gram of tissue weight (% dose/g). In separate experiments, the effects of pretreatment of spermine and unlabelled **3** on the brain uptake of male Sprague–Dawley rats (10—12 weeks old) were investigated. The drugs (7 μmol/kg) were injected intravenously 10 min before injection of [^{11}C]**3** and the rats were killed at 30 min after the injection of [^{11}C]**3**. The brain was removed, dissected and regional radioactivity was determined as described above. The control rats were treated with a water solution under identical conditions.

***In Vivo* Brain Distribution in Monkey** An awake-behaving Rhesus monkey (male, 5 kg) was chaired and the head was fixed with a specifically designed head-hold device. All animal PET scans were performed with a high-resolution SHR-7700 PET camera (Hamamatsu Photonics, Shizuoka, Japan) in the same manner as described in the literature.[27] After transmission scans for attenuation correction, a dynamic emission scan in 2D acquisition mode was performed for 90 min (1 min×10 scans, 2 min×20 scans, 4 min×10 scans) following the injection of [^{11}C]**3** (303 MBq, in 2 ml saline) *via* the crural vein as a single bolus. The emission scan image was reconstructed with a Hanning filter of 4 mm and circular ROIs with a 5-mm diameter were placed over the frontal and occipital cortexes, striatum, and cerebellum. The ROI values were expressed in kBq/ml, normalized to the injected radioactivity of 185 MBq, and plotted against time . A mixture of unlabelled **3** (6 μmol/kg) and [^{11}C]**3** (230 MBq) in saline (3 ml) was injected into the same monkey to deter-

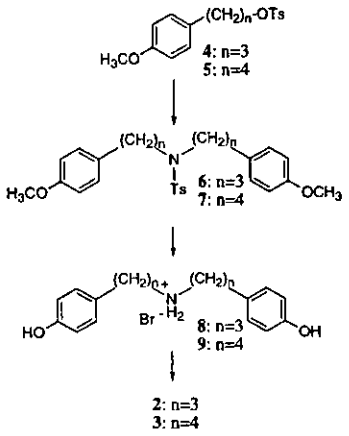

Chart 1. Synthesis of Bis(hydroxyphenylalkyl)amine (**8**, **9**) and Their Methylated Derivatives (**2**, **3**)

mine specific binding. The time activity curves in the ROIs were obtained for each scan of the brain.

RESULTS AND DISCUSSION

The synthesis was started with the tosylate (**4** or **5**), which was reacted with *p*-toluenesulfonamide in the presence of NaH in DMF to produce a dialkylated product (**6** or **7**), as described in Chart 1. The methyl protecting groups of **6** and **7** were cleaved by treatment with HBr/AcOH in the presence of phenol to give the diphenols (**8**, **9**), respectively. After neutralization with $NaHCO_3$, the free amines of the diphenol compounds (**8**, **9**) were used for the synthesis of **2** and **3**, respectively, as well as for the ^{11}C-methylation.

The radiosynthesis of [^{11}C]**2** and [^{11}C]**3** proved straightforward using standard *O*-methylation on the corresponding diphenol precursors (**8**, **9**) with [^{11}C]CH_3I in the presence of four equivalents of NaH in DMF. This can be attributed to the fact that the phenoxide group generated under basic conditions is a stronger nucleophile than the secondary amino group. Purification by reversed phase HPLC afforded [^{11}C]**2** and [^{11}C]**3** with more than 98% radiochemical purity, free from starting precursors. The specific radioactivity was estimated by UV spectroscopy to be around 75 GBq/μmol at the end of synthesis. Although the reaction conditions have not been optimized, the averages 1.2 GBq of [^{11}C]**2** and 1.6 GBq of [^{11}C]**3** after a 10 min proton bombardment at a beam current of 15 μA were obtained at end of synthesis, respectively.

In vitro bindings were initially examined by incubating the rat brain slices in a Tris HCl buffer containing [^{11}C]**2** or [^{11}C]**3**. As shown in Fig. 2, the ratios regions to cerebellum, a region free of the NR2B subunit, for the two radioligands were almost unity in all brain regions tested (cerebral cortex, hippocampus, striatum, and thalamus), thus demonstrating almost homogeneous distribution throughout the brain. Nonspecific bindings of [^{11}C]**2** and [^{11}C]**3** were about 50% and 60% of total binding, respectively, in all brain regions, as determined by the presence of the corresponding 100 μM nonradioactive ligands (Fig. 3). No significant difference in the bindings was observed between [^{11}C]**2** and [^{11}C]**3**.

The *in vitro* bindings of the ^{11}C-labelled ligands were further characterized by examining the inhibition in the frontal cortex area of the rat brain slices, which are rich in the

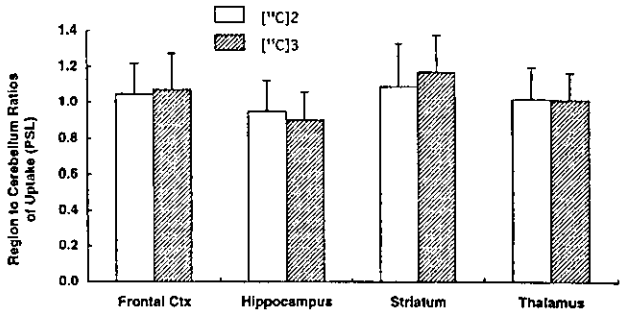

Fig. 2. Region to Cerebellum Ratios of *in Vitro* Bindings of [^{11}C]**2** and [^{11}C]**3** on Rat Brain Slices

The ratios were obtained by dividing the PSL value in each brain region by the cerebellar PSL value on the same slice and expressed as mean±S.D. (n=29 for [^{11}C]**2**, n=25 for [^{11}C]**3**).

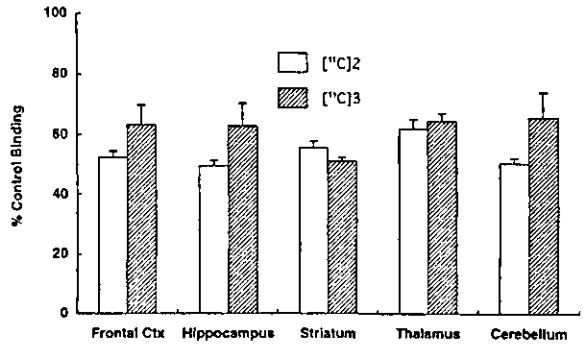

Fig. 3. Effects of Unlabelled Bis(phenylalkyl)amines (**2** or **3**, 100 μM) on the *in Vitro* Binding of [^{11}C]**2** or [^{11}C]**3** to the Rat Brain Slices

The values (mean±S.D.) were obtained by at least triplicate slices from three rats.

NMDA receptors, by various endogenous ligands related to NMDA receptors and other receptor ligands. The results of the inhibitory effects (% of control binding) are summarized in Tables 1 and 2. Among the ligands examined, ifenprodil and spermine inhibited the *in vitro* bindings with potencies similar to those of non-radioactive **2** or **3** at the same 100 μM concentration. The highly potent NR2B-selective NMDA antagonist, CP-101,606, inhibited the binding of [^{11}C]**2** and [^{11}C]**3** by only 20 and 6%, respectively, at a 10 μM concentration. It is known that ifenprodil shows equal affinities to several other CNS receptors such as σ-binding sites and α_1-adrenergic receptors.[28,29] The bindings of [^{11}C]**2** and [^{11}C]**3** to σ-binding sites and α_1-adrenergic receptors, however, were negligible by the fact that 100 μM σ- and α-antagonists did not show significant inhibition for either the [^{11}C]**2** or [^{11}C]**3** bindings. Among the polyamines, spermine showed the most potent inhibition, followed by spermidine, while putrescine showed only 10—15% inhibition even at a 1 mM concentration. These orders of inhibitory effects by polyamines are similar to those reported for the inhibition of [^{3}H]CP-101,606 and [^{3}H]ifenprodil.[30—33] Although the high-affinity ifenprodil site is supposed to be located on the NR2B subunit, a low-affinity ifenprodil site has also been proposed, through which ifenprodil acts as a weak open-channel blocker.[34] Divalent cations also inhibited the [^{11}C]**2** and [^{11}C]**3** bindings in the order of $Zn^{2+}>>Ca^{2+}>Mg^{2+}$ at their physiological concentrations. The inhibitory effects of polyamines and divalent cations have commonly been ob-